Abnormal CD8 T cells induce and track Alzheimer's-like neurodegeneration

Christopher Wheeler (chris.wheeler@brainmappingfoundation.org)
T-Neuro Pharma https://orcid.org/0000-0003-0618-8748

Akanksha Panwar
Cedars-Sinai Medical Center

Altan Rentsendorj
Cedars-Sinai Medical Center

Michelle Jhun
Cedars-Sinai Medical Center

Robert Cohen
Emory University School of Medicine

Ryan Cordner
Brigham Young Univesity

Nicole Gull
Cedars-Sinai Medical Center https://orcid.org/0000-0002-1956-5648

Robert Pechnick
Western University of Health Sciences

Gretchen Duvall
Cedars-Sinai Medical Center

Armen Mardiros
Cedars-Sinai Medical Center

David Golchian
Cedars-Sinai Medical Center

Hannah Schubloom
Cedars-Sinai Medical Center

Lee-way Jin
University of California, Davis

Debby Van Dam
University of Antwerp

Yannick Vermeiren
Institue Born-Bunge, University of Antwerp

Hans De Reu
University of Antwerp

Peter Paul De Deyn

Institue Born-Bunge, University of Antwerp

Keith Black

Cedars-Sinai Medical Center

Biological Sciences - Article

Keywords: Alzheimer's disease, neurodegeneration, CD8 T cells

Posted Date: February 26th, 2021

DOI: https://doi.org/10.21203/rs.3.rs-199647/v1

Abnormal CD8 T cells induce and track Alzheimer's-like neurodegeneration

Akanksha Panwar[a,*], Altan Rentsendorj[a,*], Michelle Jhun[a,*], Robert M. Cohen[b], Ryan Cordner[a,c,†], Nicole Gull[c], Robert N. Pechnick[d], Gretchen Duvall[a], Armen Mardiros[a,†], David Golchian[a], Hanna Schubloom[a], Lee-Way Jin[e], Debby Van Dam[f], Yannick Vermeiren[f], Hans De Reu[g], Peter Paul De Deyn[h], Keith L. Black[a], and Christopher J. Wheeler[a,i]

[a]Dept. Neurosurgery, Maxine Dunitz Neurosurgical Institute, Cedars-Sinai Medical Center, 8700 Beverly Blvd., Los Angeles, CA 90048.

[b]Dept. Psychiatry & Behavioral Sciences and Neuroscience Program, GDBBS, Emory University, 201 Dowman Dr., Atlanta, GA 30322.

[c]Dept. Biomedical & Translational Sciences, Cedars-Sinai Medical Center, 8700 Beverly Blvd., Los Angeles, CA 90048.

[d]Dept. of Basic Medical Sciences, College of Osteopathic Medicine of the Pacific, Western University of Health Sciences, 309 E. 2nd St., Pomona, CA 91766.

[e]Dept. Medical Pathology and Laboratory Medicine, M.I.N.D. Institute, University of California, Davis, 2825 50th Street, Sacramento, CA 95817.

[f]Laboratory of Neurochemistry and Behavior, Department of Biomedical Sciences, Institute Born-Bunge, University of Antwerp, Antwerp, Belgium; and
Department of Neurology and Alzheimer Research Center, University of Groningen and University Medical Center Groningen, Groningen, Netherlands.

[g]Laboratory of Experimental Hematology, Faculty of Medicine and Health Sciences, Vaccine and Infectious Disease Institute (VAXINFECTIO), University of Antwerp, Antwerp, Belgium.

[h]Laboratory of Neurochemistry and Behavior, Department of Biomedical Sciences, Institute Born-Bunge, University of Antwerp, Antwerp, Belgium; and Department of Neurology, Memory Clinic of Hospital Network Antwerp (ZNA) Middelheim and Hoge Beuken, Antwerp, Belgium; and Department of Neurology and Alzheimer Research Center, University of Groningen and University Medical Center Groningen, Groningen, Netherlands.

[i]Society for Brain Mapping & Therapeutics, Brain Mapping Foundation, Pacific Palisades, CA and T-Neuro Pharma, Inc., Albuquerque, NM & Aptos, CA, USA.

[*]These authors contributed equally to the manuscript.

[†]Present addresses: RC, Dept. of Microbiology & Molecular Biology, Brigham Young University, Provo, UT, United States; AM, Dept. of Translational Science, A2 Biotherapeutics, Inc., 30301 Agoura Road #210, Agoura Hills, CA, 91301.

Summary

Sporadic Alzheimer's disease, the most common neurodegenerative disorder of aging, is characterized by cerebral plaques and neurofibrillary tangles. Experimental rodents develop plaques but neither tangles nor substantial neurodegeneration under conditions that guarantee Alzheimer's in humans [1], suggesting rodents lack critical co-initiation factors. Accumulation of antigen-reactive memory CD8 T cells increases with aging [2], and was recently revealed as a hallmark of human Alzheimer's [3]. The impact of this process on disease initiation, however, has not been established because age-related T cell changes are muted in rodents [4-6]. We developed a mouse model of human-like CD8 T cell aging that promotes antigen-reactive memory CD8 T cell accumulation [7]. Here we show that these "^{hi}T" mice develop all major hallmarks of Alzheimer's with aging, including tangle-like inclusions and substantial neurodegeneration. Antigen-reactive CD8 T cells analogous to those in ^{hi}T mice increased in Alzheimer's brain, but decreased earlier in blood, where their loss effectively distinguished the Alzheimer's continuum from aging controls. Our findings establish a clinically relevant mouse model for sporadic Alzheimer's and show that age-related immune dysfunction critically contributes to its initiation. They also identify useful immune-based targets to track and potentially treat human Alzheimer's, while validating a model system to examine age-related disease immuno-biology more generally.

Results

Generation of "^{hi}T" cells in nude mice

We previously demonstrated that young B6.Foxn1 (B6.nude) mice injected with purified donor B6 CD8 T cells rapidly develop a T cell compartment dominated by homeostatically induced, self-reactive CD8 T cells with a resident memory phenotype ($^{hi}T_{RM}$) identical to age-related CD8 T cells accumulating in affected aged mice. This mirrors the dominance of circulating age-related memory CD8 T cells in moderate- to old-age humans [8], and rendered selected APP-reactive memory CD8 T cell levels in mice similar to those in aging humans (Extended Data Fig. E1)[9]. $^{hi}T_{RM}$ recipient mice also exhibited age-related tissue pathology, including neuroinflammation and increased memory CD8 T cells in brain, along with other factors associated with AD. We therefore examined whether B6.Foxn1 $^{hi}T_{RM}$ recipients exhibited additional neuropathological features of AD various times after T cell injection (Extended Data Fig. E2a). To ensure our observations were due to functional rather than purely physical aspects of CD8 $^{hi}T_{RM}$ accumulation in the brain, we included B6.Foxn1 cohorts injected with PBS, and with CD8 T cells from wild-type, Perforin 1-deficient, or IFNγ-deficient donors, (PBS, wt-CD8, PrfKO-CD8, and IfnγKO-CD8 groups, respectively).

Aβ and neurofibrillary deposition

CD8 T cells expanded in circulation of all B6.Foxn1 recipients [7]. By contrast, Amyloid Precursor Protein (APP) and its cleavage products including Aβ were dramatically increased only in brains of wt-CD8 group mice 3 weeks after injection (Fig. 1). Detergent-soluble Aβ1-40, but not Aβ1-42, was also elevated 10 weeks post-injection in ELISA analysis, and Western blot confirmed

prominent involvement of hippocampus at this time point (Fig. 1a, b; Extended Data Fig. E2b). By 6 months post-injection, increased Aβ deposition in brain vasculature was evident in wt-CD8 group mice, consistent with selective elevation of Aβ1-40 (Extended Data Fig. E2c). At 15 months post-injection, Aβ1-40 was still significantly elevated in wt-CD8 brain (Fig. 1b), and Aβ plaques were evident in entorhinal cortex, hippocampus, and cingulate cortex of wt-CD8 and IfnγKO-CD8 groups (Fig. 1c, d). Unlike mice expressing familial gene mutations found in human AD, Aβ plaques in both these groups were mainly diffuse and detergent-soluble (Extended Data Fig. E3a, b), with little co-staining by curcumin or ThioS (Fig. 1c; Extended Data Fig. E4a, b). The discrete amyloid pathology in the wt-CD8 group encouraged examination of additional AD-associated features such as tau phosphorylation and aggregation.

Detergent-soluble phospho-tau (pTau) was slightly (30%) but significantly increased by 10 weeks post-injection in wt-CD8 group forebrain, while pTau paired helical filaments (PHFs, which mature to form NFTs in AD) were increased nearly 5-fold (Fig. 1e). Soluble pTau did not remain elevated 15 months post-injection, however, while PHFs remained significantly elevated, but at lower than earlier levels (2.5-fold decreased; Fig. 1f). We speculated this could be due conversion of pTau isoforms to more insoluble aggregated species after 10 weeks. Indeed, fibril-staining reagents, including curcumin and Thio-S, revealed cellular inclusions within wt-CD8 group hippocampus 6 months post-injection (Extended Data Fig. E4a, b). These inclusions were apparent before larger amyloid deposits appeared, although small plaques were occasionally associated with them (Extended Data Fig. E4a, b), and were absent from aged AD-transgenic mice, as well as from AD-transgenic rats that reportedly accumulate PHFs (Extended Data Fig. E4a, b)[10].

Gallyas staining also revealed discrete silver-stained cellular structures in wt-CD8 and IfnγKO-CD8 hippocampus and cortex 15 months post-injection, that were not seen in AD-transgenic mice (Fig. 1g, h). These structures appeared similar to NFTs from human AD patients (Extended Data Fig. E5a, b). In addition, sequential staining revealed that Gallyas-stained structures in wt-CD8 and IfnγKO-CD8 groups were derived from $pTau^+$ neurons with intact nuclei (Fig. 1g), and that Gallyas and pTau staining was superimposable and distinct from that of Aβ (Fig. 1g; Extended Data Fig. E5c). "Ghost tangles", NFTs in dead neurons that are often present in human AD [11,12], were not observed. These data suggest that $^{hi}T_{RM}$ promote the coordinated deposition of parenchymal Aβ40, diffuse plaques, and fibrillar pTau inclusions in live neurons, either directly or by indirectly promoting neuroinflammation.

Immune & neuroinflammatory infiltration

Our previous work established that astrogliosis, microgliosis, and CD8 T cell brain infiltration were all increased in wt-CD8 group $^{hi}T_{RM}$ hosts [7]. We therefore examined the relationship of observed neuroinflammatory features to Aβ plaque burden to determine the immune population most directly associated with neuropathology. Aβ plaque burden correlated strongest with hippocampal CD8 T cell numbers compared to astrogliosis or microgliosis, consistent with a more direct impact of adaptive than innate immune cells on amyloid pathology (Extended Data Fig. E6). In this context, it is intriguing that, while PrfKO-CD8 group mice failed to exhibit either CD8 T cells in brain, or any significant AD-like neuropathology, IfnγKO-CD8 group mice retained significantly increased plaques and NFT-like structures in hippocampus and entorhinal cortex, but not in cingulate cortex (Fig. 1d, h). This resembles the distribution of protein aggregates early in human AD [13], and as such suggests that neuroinflammation hastens AD-like neuropathology in

$^{hi}T_{RM}$ mice, but is not required for its development. Taken together, our data suggest that $^{hi}T_{RM}$ may directly promote pathologic features of AD-like neurodegeneration.

Neuronal loss & cerebral atrophy

Robust neurodegeneration is not present in mouse AD models without addition of transgenes uninvolved in human AD [1,14]. To determine if overt neurodegeneration was present in $^{hi}T_{RM}$ mice, we stained and counted $NeuN^+$ neurons in CA1, CA2, and CA3 of hippocampus, assessed brain mass, and quantified Western blots of NeuN and synaptic proteins. Loss of $NeuN^+$ cells in wt-CD8 group mice was visually apparent in hippocampal immunostains, and was verified by $NeuN^+$ cell counts at 15 months post-injection (Fig. 2a-c). Loss of brain mass was also evident in wt-CD8 group, and progressed from 5% at 6 months, to 10% 15 months post-injection (Fig. 2d), which is comparable to terminal brain atrophy in human AD [15]. Western blots confirmed an approximate 10% decrease in NeuN, as well as in the synaptic protein, Drebrin, and a non-significant trend toward lower Synaptophysin protein, 15 months post-injection (Fig. 2e, f). Importantly, loss in brain mass correlated with decreased NeuN across all T cell injection groups, establishing a direct relationship between brain mass and neuronal loss (Fig. 2g). Thus, B6.nude $^{hi}T_{RM}$ recipients exhibited robust and easily discernible neurodegeneration by multiple measures, with related brain atrophy. This revealed the possibility that $^{hi}T_{RM}$ mice might exhibit AD-like dementia as well.

Severe cognitive impairment

Prior to cognitive testing in $^{hi}T_{RM}$ mice, we established that spontaneous locomotor activity was not significantly different between treatment and control groups in Open Field testing 3, 6, and 13 months after T cell injection (Fig, 3a; Extended Data Fig. E7a), ruling out motor deficits such as those in multiple sclerosis. Nevertheless, all groups exhibited motor deficits that increased with

age, but this was unrelated to treatment. In contrast to motor activity, Fear Conditioning (FC) response to contextual but not cued learning was reduced in wt-CD8 group mice 6 months after T cell injection, with both contextual and cued learning impaired in the same mice tested 5 months later (Fig 3b). The hippocampus is required for contextual FC responses, whereas both hippocampus and amygdala are required for cued FC responses. Hence, the FC results suggest that $^{hi}T_{RM}$ mediate damage to hippocampus alone early on, and cause further damage to amygdala later, a pattern commonly seen in human AD [16]. Contextual performance at 6 and 11 months also correlated with brain mass (Extended Data Fig. E7b), further underscoring the relationship of cognitive decline to physical neurodegeneration.

Spontaneous Alternation Behaviour (SAB) 12 months post-injection independently confirmed behavioral abnormalities in wt-CD8 group mice exclusively. This test is based on the preference of mice to alternately explore two alleys, which requires working memory of the alley previously entered. The lowest possible score of 50% indicates random alley choice, reflecting either no working memory, or complete lack of preference. The 55-56% SAB score in the PBS group was comparable to published wild-type values [17], but the wt-CD8 group SAB was significantly lower at 50% (Fig. 3c). To verify whether this reflected loss of working memory or lack of preference, we employed the Barnes Maze test at 14 months, a more focused measure of hippocampus-dependent learning and memory. In contrast to all other groups, wt-CD8 mice showed no ability to learn the maze over the initial 4-day training period, indicating a profound learning and memory deficit (Fig. 3d). Given this inability, wt-CD8 mice were uniquely impaired on subsequent memory retention and reversal phases of the maze as well (Fig. 3e-g). As with Fear-Conditioning, latency to solve the Barnes Maze correlated inversely with brain mass (Extended Data Fig. E7c). Taken

together, these tests suggest that fully functional $^{hi}T_{RM}$ mediate severe, progressive impairment of hippocampus-dependent learning and memory, but not locomotor activity.

Because cognitive impairment is differentially associated with amyloid and tau pathology in AD, we further addressed whether cognitive loss was associated with Aβ and/or pTau metrics in $^{hi}T_{RM}$ mice. Poor performance on Barnes Maze (total latency below median = BM^{lo}) exhibited significant association only with increased pTau PHFs on Western blots (Extended Data Fig. E7d), and not with Triton-soluble or GuanidineHCl-soluble Aβ1-40 or Aβ1-42 on ELISA, or with detergent soluble pTau by Western blot (Extended Data Fig. E7e, f). Thus, cognitive impairment appeared preferentially associated with fibrillar tau pathology in wt-CD8 group mice, as it is in human AD [18].

^{hi}T cell metrics in Alzheimer's disease

To examine possible involvement of T cells analogous to those in $^{hi}T_{RM}$ mice in AD, we quantified CD8 T cells in blood, their relationship to cognitive decline, and their presence in brain, using three human cohorts (Fig. 4a). We first examined $KLRG1^+$ and $KLRG1^-$ CD8 T cell subpopulations in blood from aging control subjects (CTRL), MCI patients with an AD-typical CSF biomarker profile (MCI-AD), MCI patients without an AD-typical CSF biomarker profile (MCI), and sporadic AD patients (AD) (Cohort 1). $KLRG1^+$ CD8 T cells were not significantly increased in AD blood (Fig. 4b), but increased in rough correlation with age, while $KLRG1^-$ CD8 T cells did not (Extended Data Fig. E8). In contrast, $KLRG1^+$ CD8 T cells co-stained with pHLA-A2 multimers to a human T cell epitope analogous to that recognized by T cells in $^{hi}T_{RM}$ mice [$APP_{(471-479)}$] were dramatically decreased in the blood of MCI, MCI-AD, and AD patients (Fig. 4c, d). While this differs from other (i.e., EBV-specific) CD8 T cells that increase in AD [3],

segregation of CTRL and MCI patients by cognitive performance score did reveal that KLRG1$^+$ CD8 T cells increased during age-related cognitive decline (Fig. 4d). Moreover, $APP_{(471-479)}$-specific KLRG1$^+$ CD8 T cell levels correlated significantly with cognitive decline but not age itself (Fig. 4e). The parental KLRG1$^+$ CD8 T cell population thus appears to expand in blood earlier than other memory CD8 T cells [3], and appears to contract as cognitive decline is clinically diagnosed. This could conceivably prompt compensatory expansion by cells such as T_{EMRA} to occupy a depleted memory CD8 T cell pool (Extended Data Fig. E8).

Decreased KLRG1$^+$ $APP_{(471-479)}$-specific CD8 T cells in blood distinguished AD from normal aging patients with less overlap than another promising blood-based biomarker for AD in development, plasma levels of P-Tau217 (Extended Data Fig. E9a, b)[19]. Diagnostic potential of this decrease was indicated in Receiver Operating Characteristic (ROC) analysis, where it effectively distinguished AD and AD-related MCI from CTRL blood (Extended Data Fig. E9c). Specifically, area under the curve (AUC) for AD-related MCI and AD were 0.865 and 0.892, respectively, with AD-unrelated MCI AUC = 0.760 (Extended Data Fig. E9c).

We next examined CD8 and Perforin-1 content in AD brain. Importantly, Western blots rendered the expected antibody specificities (68-75 kDa Prf1; 33-35 kDa CD8α), with anti-Prf1 staining lymphocytic nuclei with the expected punctate pattern (Fig. 4f). Perforin1 and CD8 Western signals were correlated (n = 6; r = 0.8155, $P = 0.048$; not shown), and both were increased in AD cortex, with Perforin1 reaching statistical significance (Fig. 4g). This is consistent with elevated cytolytic CD8 T cells in AD brain. To examine this more directly, we stained hippocampal sections from AD patients and normal aging controls by tissue immunofluorescence and quantified cells stained with anti-CD8 alone or co-stained with $APP_{(471-479)}$-/HLA-A2 multimers (Fig. 4h). As in $^{hi}T_{RM}$ mice, total CD8 T cells were not significantly elevated in AD brain (n = 10; 1.6 $\pm$ 0.29 vs.

207 2.3 $\pm$ 0.55, P = 0.31; not shown). Nevertheless, APP-specific CD8 T cells were increased in
208 perivasculature and cortical regions of AD hippocampus (Fig. 4i), similar to $^{hi}T_{RM}$ mice and as
209 predicted by that model.

210 Conclusion

211 In conclusion, we show for the first time that all major hallmarks of human AD can be elicited by
212 a single inductive event in mice. This pathology is dependent on expansion in blood and entry into
213 brain of age-related resident memory CD8 T cells (CD8 T_{RM}), and exhibits gross similarity to
214 human AD with important distinctions. Notably, amyloidopathy in $^{hi}T_{RM}$ mice was limited to Aβ1-
215 40 and mainly diffuse plaques, unlike the Aβ1-42 and mature neuritic plaques that predominate in
216 many AD patients. Moreover, while $^{hi}T_{RM}$ mice exhibited fibrillar NFT-like structures in live cells,
217 they did not harbor the ghost tangles in dead neurons often seen in human AD. While Aβ
218 differences could reflect deficiencies in Aβ1-42 clearance and/or fibril formation characteristic of
219 rodent brains [20,21], the lack of ghost tangles is likely due to decreased expression in adult mice of
220 the ghost tangle-promoting isoforms of MAPT, the gene encoding tau proteins [11,12].
221
222 Despite these distinctions, $^{hi}T_{RM}$ mice exhibited unique similarities to sporadic AD in humans
223 beyond amyloidosis, fibrillar tauopathy, and robust neurodegeneration. These included cognitive
224 decline that initiated with hippocampus-dependent tasks with later progression to amygdala-
225 dependent tasks [16]; significant association of cognitive loss exclusively with fibrillar tau pathology
226 [18]; neuroinflammation that exacerbated neuropathology [22]; and accumulation of antigen-specific
227 memory CD8 T cells in brain [7], the most recently characterized hallmark of human AD [3]. The
228 pattern of ample NFT-like structures, vascular amyloidosis, Aβ1-40 and diffuse plaque

predominance seen in $^{hi}T_{RM}$ mice also resembled that of at least one subpopulation of human AD patients in carriers of the APP Iowa mutation [23,24].

CD8 T cells reactive to an antigenic epitope nearly identical to that recognized by brain-localized T cells in $^{hi}T_{RM}$ mice, were increased in AD brain but decreased in AD and MCI blood, suggesting that their movement from blood to brain is involved in neuropathology. Consistent with this notion, decreased levels of KLRG1$^+$ APP$_{(471-479)}$/HLA-A2 multimer-binding CD8 T cells in blood correlated with cognitive impairment in MCI patients. While somewhat reminiscent of a distinct subpopulation of CD8 effector-memory T cells, T_{EMRA}, $^{hi}T_{RM}$ analogues are distinct in that they were weakly age-related, their decrease rather than increase correlated with cognitive loss, and were prominently reactive to self antigen [3]. T_{EMRA} are also absent from mice [3,25,26]. Further contrasting these subpopulations. Finally, CD8 T_{RM} expanded during age-related cognitive decline, a stage that precedes MCI when T_{EMRA} are reported to expand. Thus, CD8 T_{RM} alterations occur earlier are unique with respect to those of T_{EMRA}, and may be more direct beacons of AD induction than other immune or non-immune factors in blood.

Accordingly, levels of KLRG1$^+$ HLA-A2/APP$_{(471-479)}$-specific CD8 T cells in blood distinguished AD from normal aging patients with significantly less overlap than plasma P-Tau217, a blood-based biomarker met with much enthusiasm (Extended Data Fig. E9a, b)[19], and tracked AD and AD-related MCI with high accuracy (Extended Data Fig. E9c). Further assessment of the potential of $^{hi}T_{RM}$ metrics as diagnostic biomarkers for AD requires multi-center validation, as well as prospective and longitudinal analyses with non-AD dementia cohorts. From a therapeutic perspective, it will be equally important to determine whether modulation of antigen-specific $^{hi}T_{RM}$ presence or function can alter the course of AD-like neurodegeneration in mice, and determine if effective treatments for AD critically modulate these cells in humans. Finally, continued

examination of $^{hi}T_{RM}$ mice on multiple strain backgrounds, and harboring various risk factors for AD and distinct age-related disorders, may lead to a more comprehensive understanding of their biology, genetics, and immune features.

References:

1 Schwab, C., Hosokawa, M. & McGeer, P. L. Transgenic mice overexpressing amyloid beta protein are an incomplete model of Alzheimer disease. *Exp Neurol* **188**, 52-64 (2004).

2 Ritzel, R. M. *et al.* Age-Associated Resident Memory CD8 T Cells in the Central Nervous System Are Primed To Potentiate Inflammation after Ischemic Brain Injury. *J Immunol* **196**, 3318-3330, doi:10.4049/jimmunol.1502021 (2016).

3 Gate, D. *et al.* Clonally expanded CD8 T cells patrol the cerebrospinal fluid in Alzheimer's disease. *Nature* **577**, 399-404, doi:10.1038/s41586-019-1895-7 (2020).

4 Clambey, E. T., van Dyk, L. F., Kappler, J. W. & Marrack, P. Non-malignant clonal expansions of CD8+ memory T cells in aged individuals. *Immunol Rev* **205**, 170-189 (2005).

5 Clambey, E. T., White, J., Kappler, J. W. & Marrack, P. Identification of two major types of age-associated CD8 clonal expansions with highly divergent properties. *Proc Natl Acad Sci U S A* **105**, 12997-13002 (2008).

6 den Braber, I. *et al.* Maintenance of peripheral naive T cells is sustained by thymus output in mice but not humans. *Immunity* **36**, 288-297, doi:10.1016/j.immuni.2012.02.006 (2012).

7 Panwar, A. *et al.* Functional recreation of age-related CD8 T cells in young mice identifies drivers of aging- and human-specific tissue pathology. *Mech Ageing Dev* **191**, 111351, doi:10.1016/j.mad.2020.111351 (2020).

8 Schwab, R. *et al.* Expanded $CD4^+$ and $CD8^+$ T cell clones in elderly humans. *J Immunol* **158**, 4493-4499 (1997).

9 Nikolich-Zugich, J., Li, G., Uhrlaub, J. L., Renkema, K. R. & Smithey, M. J. Age-related changes in CD8 T cell homeostasis and immunity to infection. *Semin Immunol* **24**, 356-364, doi:10.1016/j.smim.2012.04.009 (2012).

10 Cohen, R. M. *et al.* A transgenic Alzheimer rat with plaques, tau pathology, behavioral impairment, oligomeric abeta, and frank neuronal loss. *J Neurosci* **33**, 6245-6256, doi:10.1523/jneurosci.3672-12.2013 (2013).

11 Lace, G. *et al.* Hippocampal tau pathology is related to neuroanatomical connections: an ageing population-based study. *Brain : a journal of neurology* **132**, 1324-1334, doi:10.1093/brain/awp059 (2009).

12 Uchihara, T., Hara, M., Nakamura, A. & Hirokawa, K. Tangle evolution linked to differential 3- and 4-repeat tau isoform deposition: a double immunofluorolabeling study using two monoclonal antibodies. *Histochem Cell Biol* **137**, 261-267 (2012).

13 Reitz, C., Honig, L., Vonsattel, J. P., Tang, M. X. & Mayeux, R. Memory performance is related to amyloid and tau pathology in the hippocampus. *Journal of neurology, neurosurgery, and psychiatry* **80**, 715-721, doi:10.1136/jnnp.2008.154146 (2009).

14 Codita, A., Winblad, B. & Mohammed, A. H. Of mice and men: more neurobiology in dementia. *Curr Opin Psychiatry* **19**, 555-563 (2006).

15 Sluimer, J. D. *et al.* Whole-brain atrophy rate and cognitive decline: longitudinal MR study of memory clinic patients. *Radiology* **248**, 590-598 (2008).

16 Serrano-Pozo, A., Frosch, M. P., Masliah, E. & Hyman, B. T. Neuropathological alterations in Alzheimer disease. *Cold Spring Harbor perspectives in medicine* **1**, a006189, doi:10.1101/cshperspect.a006189 (2011).

17 Ma, Q. L. *et al.* Beta-amyloid oligomers induce phosphorylation of tau and inactivation of insulin receptor substrate via c-Jun N-terminal kinase signaling: suppression by omega-3 fatty acids and curcumin. *J Neurosci* **29**, 9078-9089 (2009).

18 Brier, M. R. *et al.* Tau and Abeta imaging, CSF measures, and cognition in Alzheimer's disease. *Science translational medicine* **8**, 338ra366, doi:10.1126/scitranslmed.aaf2362 (2016).

19 Palmqvist, S. *et al.* Discriminative Accuracy of Plasma Phospho-tau217 for Alzheimer Disease vs Other Neurodegenerative Disorders. *JAMA* **324**, 772-781, doi:10.1001/jama.2020.12134 (2020).

20 Banks, W. A., Robinson, S. M., Verma, S. & Morley, J. E. Efflux of human and mouse amyloid beta proteins 1-40 and 1-42 from brain: impairment in a mouse model of Alzheimer's disease. *Neuroscience* **121**, 487-492 (2003).

21 Shin, R. W. *et al.* Amyloid beta-protein (Abeta) 1-40 but not Abeta1-42 contributes to the experimental formation of Alzheimer disease amyloid fibrils in rat brain. *J Neurosci* **17**, 8187-8193 (1997).

22 Liang, K. Y. *et al.* Exercise and Alzheimer's disease biomarkers in cognitively normal older adults. *Ann Neurol* **68**, 311-318, doi:10.1002/ana.22096 (2010).

23 Grabowski, T. J., Cho, H. S., Vonsattel, J. P., Rebeck, G. W. & Greenberg, S. M. Novel amyloid precursor protein mutation in an Iowa family with dementia and severe cerebral amyloid angiopathy. *Ann Neurol* **49**, 697-705 (2001).

24 Hellstrom-Lindahl, E., Viitanen, M. & Marutle, A. Comparison of Abeta levels in the brain of familial and sporadic Alzheimer's disease. *Neurochemistry international* **55**, 243-252, doi:10.1016/j.neuint.2009.03.007 (2009).

25 Pangrazzi, L. *et al.* Increased IL-15 Production and Accumulation of Highly Differentiated CD8(+) Effector/Memory T Cells in the Bone Marrow of Persons with Cytomegalovirus. *Frontiers in immunology* **8**, 715, doi:10.3389/fimmu.2017.00715 (2017).

26 Willinger, T., Freeman, T., Hasegawa, H., McMichael, A. J. & Callan, M. F. Molecular signatures distinguish human central memory from effector memory CD8 T cell subsets. *J Immunol* **175**, 5895-5903, doi:10.4049/jimmunol.175.9.5895 (2005).

27 West, M. J., Slomianka, L. & Gundersen, H. J. G. Unbiased stereological estimation of the total number of neurons in the subdivisions of the rat hippocampus using the optical fractionator. *The Anatomical Record* **231**, 482-497, doi:10.1002/ar.1092310411 (1991).

28 Bach, M. E., Hawkins, R. D., Osman, M., Kandel, E. R. & Mayford, M. Impairment of spatial but not contextual memory in CaMKII mutant mice with a selective loss of hippocampal LTP in the range of the theta frequency. *Cell* **81**, 905-915, doi:10.1016/0092-8674(95)90010-1 (1995).

29 Pitts, M. W. Barnes Maze Procedure for Spatial Learning and Memory in Mice. *Bio-protocol* **8**, doi:10.21769/bioprotoc.2744 (2018).

30 Engelborghs, S. *et al.* Diagnostic performance of a CSF-biomarker panel in autopsy-confirmed dementia. *Neurobiol Aging* **29**, 1143-1159, doi:10.1016/j.neurobiolaging.2007.02.016 (2008).

31 Petersen, R. C. Mild cognitive impairment as a diagnostic entity. *Journal of internal medicine* **256**, 183-194, doi:10.1111/j.1365-2796.2004.01388.x (2004).

32 McKhann, G. M. *et al.* The diagnosis of dementia due to Alzheimer's disease: recommendations from the National Institute on Aging-Alzheimer's Association

workgroups on diagnostic guidelines for Alzheimer's disease. *Alzheimers Dement* **7**, 263-269, doi:10.1016/j.jalz.2011.03.005 (2011).

33 Dubois, B. *et al.* Advancing research diagnostic criteria for Alzheimer's disease: the IWG-2 criteria. *Lancet Neurol* **13**, 614-629, doi:10.1016/s1474-4422(14)70090-0 (2014).

Figure Legends

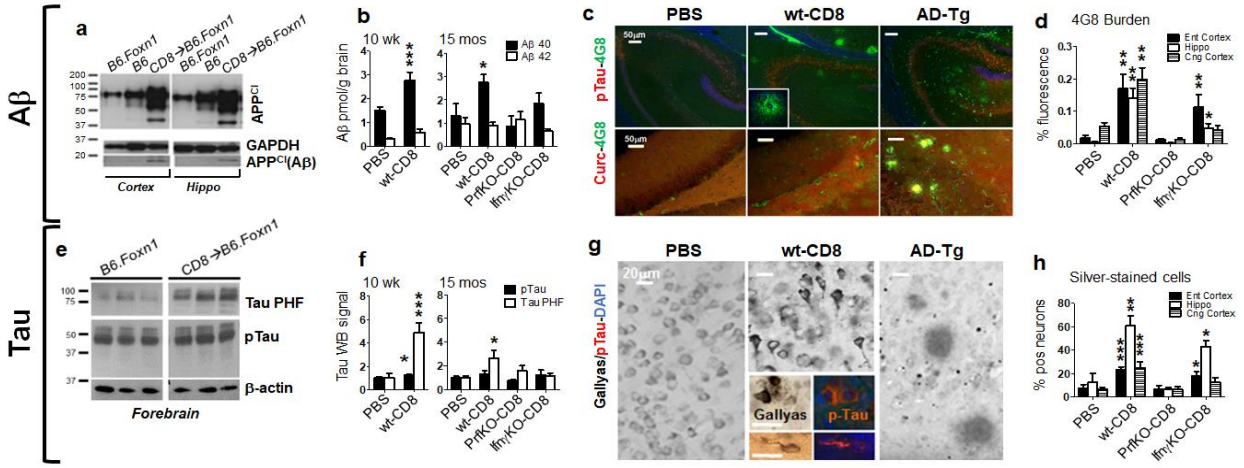

Fig. 1: Amyliod and pTau pathology. Western blots of APP cleavage products (APP^{Cl}) in cortex, hippocampus 3 wk after injection (→) of recipients **(a)**. **B-J** depict B6.Foxn1 recipients , 15 mos post-injection unless otherwise indicated. Forebrain Aβ1-40/42 ELISA **(b)**. Plaques ± pTau/curcumin staining **(c)**, and compiled 4G8 burden in entorhinal (Ent)/cingulate (Cng) cortex, and hippocampus (Hippo) **(d)**. Western blots **(e)**, and compiled pTau and PHF signal. Gallyas/silver-stained cells in $^{hi}T_{RM}$ groups and 18-month-old Tg2576 (AD-Tg) mice**,** with sequential pTau→Gallyas stains inset **(g)**. $Gallyas^{+}$ neuron **(h)** percentages Plots depict averages ± SEM. $*P < 0.05$, $**P < 0.01$, $***P < 0.005$ by 2-sided T-test, relative to PBS group.

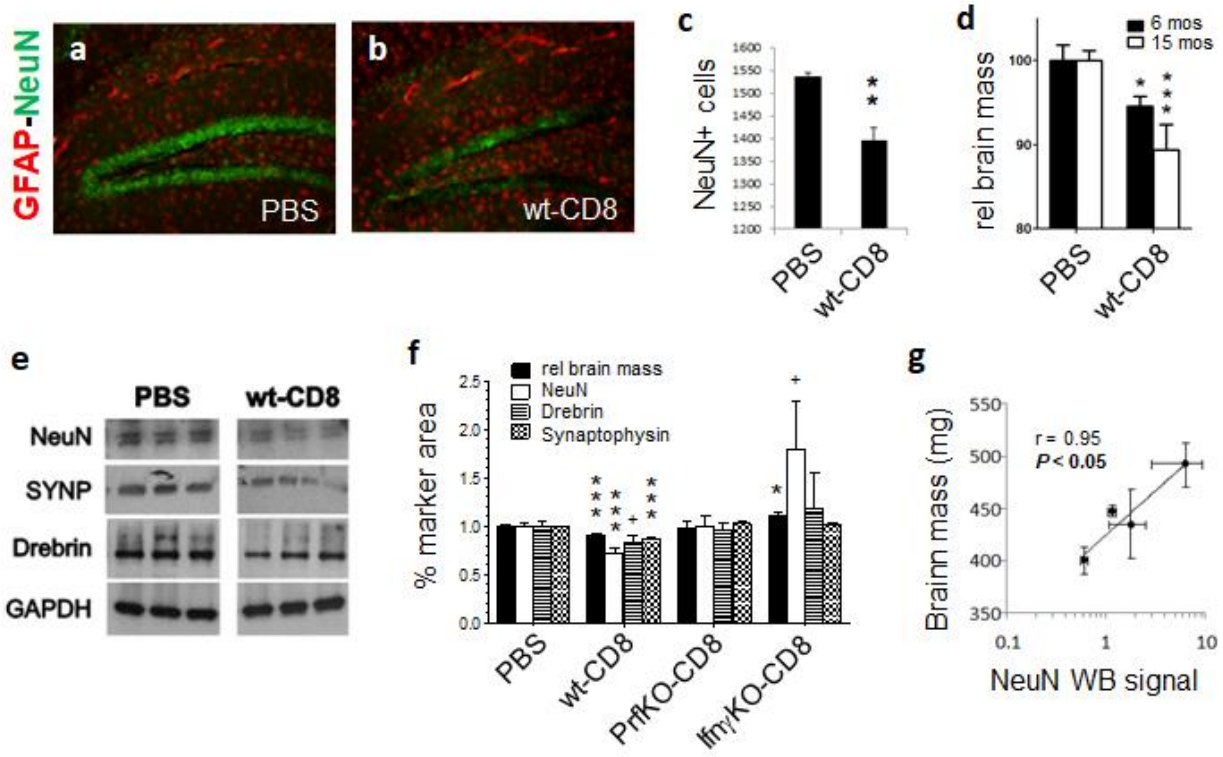

363

364 **Fig. 2: Neurodegeneration in nude mice harboring ^{hi}T cells.** Cell/control recipients in all panels
365 are B6.Foxn1 exclusively. NeuN and GFAP staining **(a, b)**, and cell counts in hippocampus, 15
366 mos after cell/control injection **(c)**. Brain atrophy over time in PBS and wt-CD8 groups (mass
367 normalized to PBS controls at each time point; **d)**. Representative forebrain Westerns (**e**), and
368 GAPDH-normalized NeuN, Drebrin, and Synaptophysin Western signals (**f**). Correlation of NeuN
369 with brain weight (**g**). Plots depict averages ± SEM. **P* < 0.05, ***P* < 0.01, ****P* < 0.005 by 2-
370 sided T-test, relative to PBS group.

371

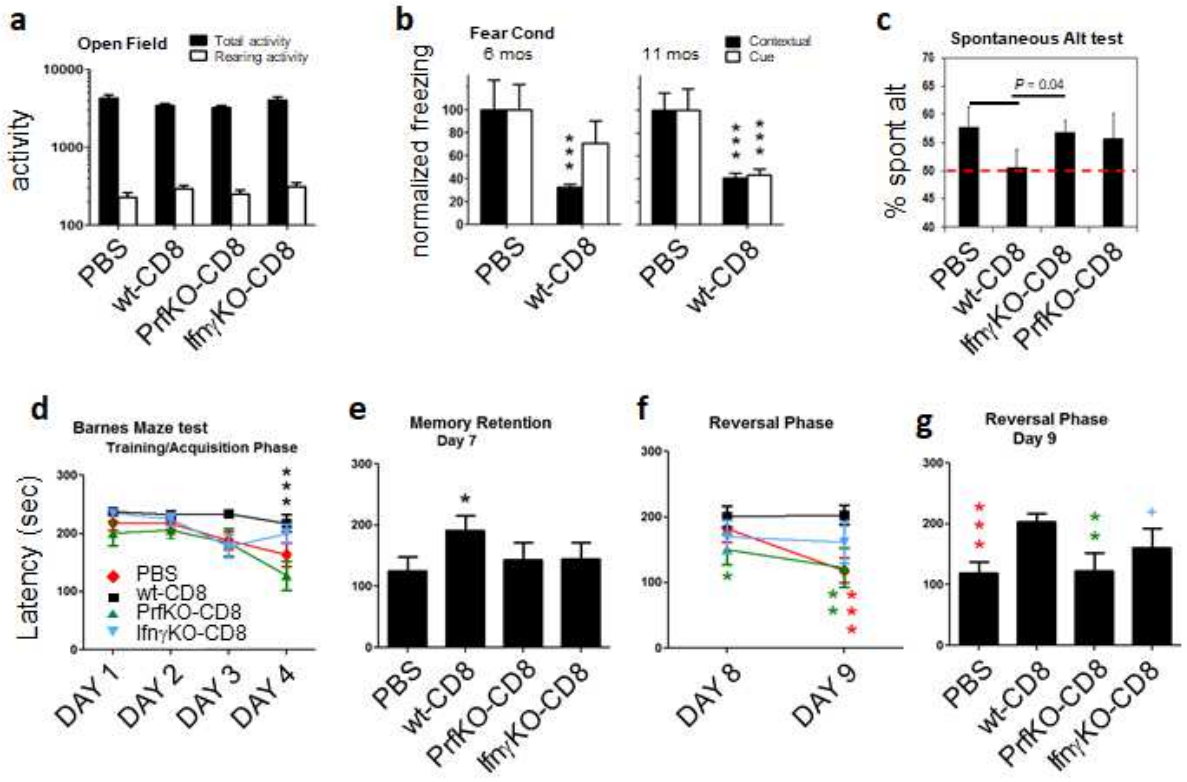

372

373 **Fig. 3: Cognition in nude mice harboring ^{hi}T cells.** Representative Open Field test at 13 mos
374 **(a)**. Fear Conditioning over time **(b)**, and Spontaneous Alternation Behavior at 12 months **(c)**.
375 Barnes Maze learning/training **(d)**, retention **(e)**, and reversal **(f, g)** phases, at 14 mos (black,
376 colored symbols = *P* relative to PBS, wt-CD8, respectively). Plots depict averages ± SEM. **P* <
377 0.05, ***P* < 0.01, ****P* < 0.005 by 2-sided ANOVA (panel **d**) or 2-sided T-test (all others), relative
378 to PBS group unless otherwise indicated.

379

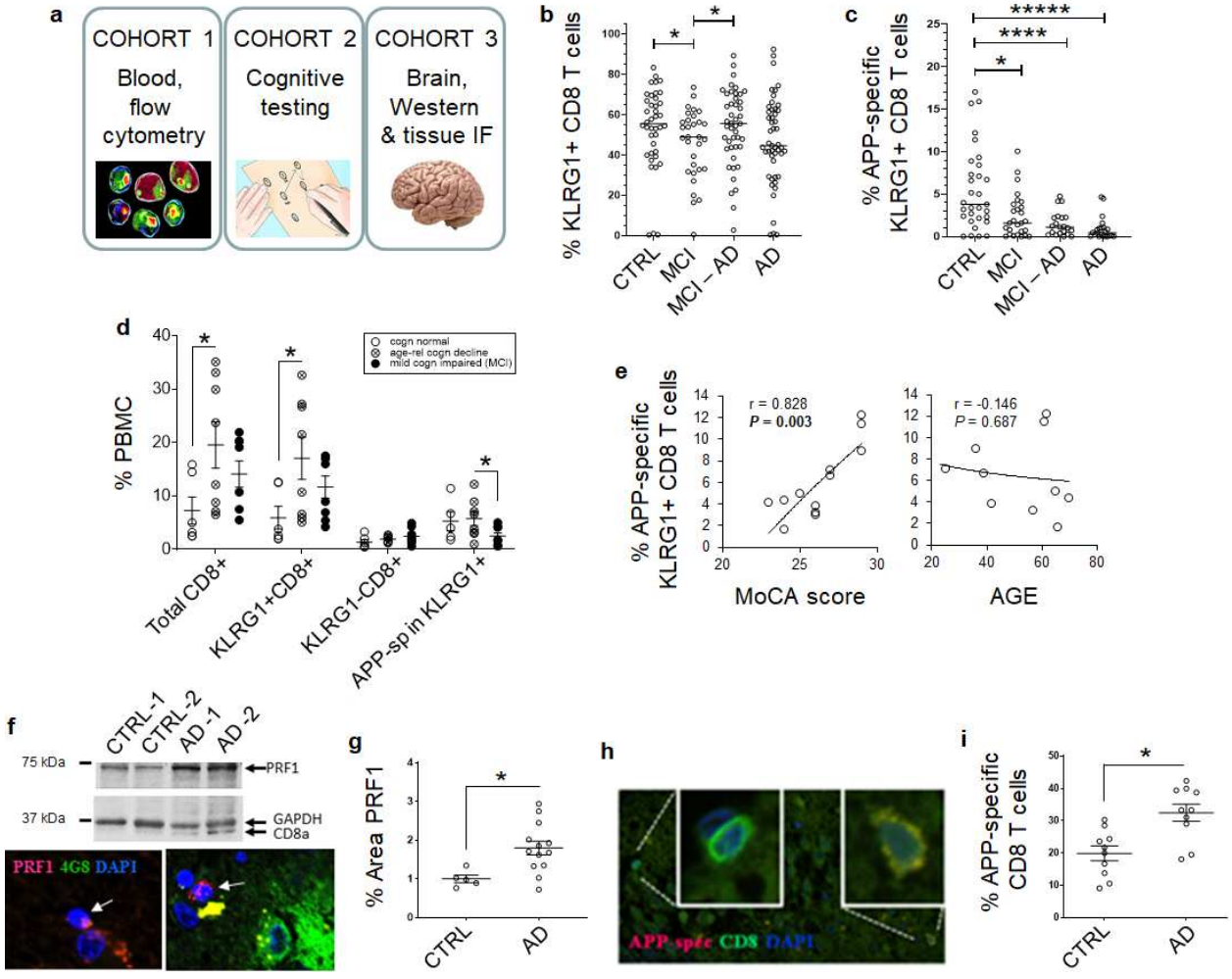

Fig. 4: ^{hi}T parameters in human Alzheimer's. Patient cohorts (**a**). KLRG1^{+} (**b**) and APP$_{(471-479)}$/HLA-A2-reactive KLRG1^{+} (**c**) CD8 T cells in CTRL, MCI ± CSF AD biomarkers (MCI, MCI–AD), and verified Alzheimer's (AD) blood. T cell subpopulations vs. MoCA score (**d**), and correlation of APP$_{(471-479)}$/HLA-A2-reactive KLRG1^{+} CD8 with score and age (**e**). PRF1 Western blot and immunofluorescence **(f)**, with quantifications in age-matched CTRL and AD brains. **(g)**. APP$_{(471-479)}$/HLA-A2-reactive CD8 staining (**h**) and quantification (**i**) in brain. Plots depict

388 averages ± SEM. *$P < 0.05$, **$P < 0.01$, ***$P < 0.005$, ****$P < 0.001$ by 2-sided T-test, relative

389 to CTRL unless otherwise indicated.

390

Methods

Animal subjects

Female C57BL/6, B6.Foxn1 mice, and congenic and/or syngeneic knockout strains (Jackson Labs) were housed in a pathogen–free vivarium under standard conditions on a 12-h light/12-h dark cycle with food and water *ad libitum.* Recipient animals were 8-10 week-old female B6.Foxn1, B6.Foxn1-AppKO, or B6.CD45.1-congenic mice; donors were 5-8 week-old females of the same strains. Specific numbers of animals used for all analytical methods are included in Supplemental Table 1. Cell derivation was randomized by pooling from $\geq$5 donors per experiment. Young (8-10 wk) and aged (15 months) male and female C57BL/6 and B6.CD103-knockout mice (n = 12 young; n = 7-8 aged) were used to study age-related cognitive decline. Donor, recipient, and unmanipulated animals were maintained in a pathogen-free facility under the Cedars-Sinai Department of Comparative Medicine, with all breeding and genetic screening conducted at Jackson Laboratories (Bar Harbor, ME)**.**

Adoptive transfer of CD8 T cells

Splenic $CD8^+$ T cells from C57BL/6J female mice (5-7 weeks old) were purified using anti-CD8 immunobeads (Miltenyi Biotech, Sunnyvale, CA). 3 x 10^6 CD8 T cells in 50 µl of PBS were injected intravenously into female C57BL/6J or B6.Foxn1 nude hosts. Transfer efficiency into B6.Foxn1 hosts was validated by persistence of $\geq$5% $CD8^+$ T cells within splenic lymphocytes 3 weeks after injection. The order of treatments was randomized by alternating cell and control injections between individual recipients. For all subsequent analyses, performing investigators were blinded to both group definition and anticipated outcomes.

Tissue processing

Brain and spleen were harvested from mice perfused with saline under deep anesthesia using a Ketamine and Xylazine (40-50 mg/kg i.p.) cocktail, until major organs such as liver and lungs lost color, and tissue was then excised for analysis. Upon removal of the whole brain from the cranium, the cerebellum, brainstem, and olfactory bulbs were removed, and remaining brain tissue was weighed on a Mettler balance for standardized brain mass assessment. Brains were sectioned 1 mm to the right of the longitudinal fissure (midline). Right hemispheres were flash frozen in -80°C conditions for protein studies, followed by homogenization in Cell Lysis Buffer (Cell Signaling Technologies, MA), and centrifugation of nuclei. Cell lysates were separated into Triton-soluble, Sarkosyl-soluble and Sarkosyl-insoluble fractions using sequential incubations with 10% (wt/V) salt sucrose solution and 1% (wt/v) sarkosyl Salt Sucrose Solution. Left hemispheres were immersion fixed in 4% paraformaldehyde (duration?) and reserved for immunohistochemical staining.

Antibodies for tissue staining and western blot analyses

Free-floating brain sections (8-14 µm thick) were mounted onto slides and blocked with Protein Block (Serum-Free, Dako, CA) for 1h at RT. Sections were incubated at 4^{o}C overnight with primary antibody in Protein Block (Dako, CA). Sections were rinsed 4x in PBS, and incubated 90 min in fluorochrome- or biotin-conjugated secondary antibody, with or without curcumin (0.01% in PBS), or with ThioS alone (1% in PBS). Sections were washed, coverslipped, and mounted with ProLongGold anti-fade media with DAPI (Invitrogen). Bright-field and fluorescent images were obtained using a Zeiss AxioImagerZ1 with CCD camera (Carl Zeiss Micro imaging). Image analysis of micrographs was performed with ImageJ (NIH). Anti-Aβ/APP antibody

(ab14220, Abcam for 3-week time point; clone 4G8, Chemicon for all others) was used at 1:500 for immunohistochemistry (IHC) and 1:1000 for Western blot (WB). Anti-pTau pS199/202 antibody (Invitrogen) was used at 1:50 for IHC and 1:100 for WB, with PHFs confirmed with Phospho-PHF-tau pSer202+Thr205 Antibody (AT8), used at 1:2000 for WB. Due to marker size, pTau WB signal was normalized to that of β-actin (clone AC-74, Sigma), with GAPDH used for normalization of all other markers. Anti-GFAP (Dako) was used at 1:250 for IHC and WB. Anti-NeuN antibody (Chemicon) was used at 1:100 for IHC and WB. Anti-Iba1 (Wako, Ltd.) was used at 1:200 for IHC. Anti-CD8 (clone 53-6.72, BD Pharmingen) was used at1:100 for IHC and 1:1000 for WB. All secondary antibodies (HRP, Alexa Flour-488, -594, -647; Invitrogen) were used at 1:200 for IHC and 1:2000 for WB. Multimer generation & use: dextramers of established epitopes for self/brain antigen (Trp-2-$DCT_{(180\text{-}188)}$/H-$2K^b$), and/or custom APP epitopes with predicted affinities < 100nM (NetMHC version 3.4; $APP_{(470\text{-}478)}$/H-$2D^b$), were manufactured by Immudex.

Western blot for amyloid, tau, neural and immunological markers

Triton-soluble cell lysates were electrophoretically separated on 12% Tris-HCl Precast Gels (Bio-Rad), and blotted onto 0.2 µm nitrocellulose membranes. Membranes were blocked with bovine serum albumin (BSA), incubated in sequential primary and secondary antibody dilutions for 1 hr at room temperature with $\geq$3 washes, developed with enhanced chemiluminescence substrate (GE Healthcare Biosciences; Pittsburgh, PA), and exposed onto Amersham Hyperfilm (GE Healthcare Biosciences; Pittsburgh, PA).

ELISA

Supernatant from homogenized brain tissues was used for Triton-soluble Aβ. Insoluble pellets from Triton-homogenized brain were resuspended in 10 volumes 5M Guanidine HCl 4 hr to generate Guanidine-soluble Aβ. Triton- and Guanidine-soluble samples were subjected to analysis by Soluble and Insoluble Aβ ELISA (Invitrogen, Life Technologies; Grand Island, NY). Absorbance was read on a SPECTRAmax Plus384 microplate reader (Molecular Devices, Sunnyvale, CA) with data analyzed in Graphpad PRISM (Graphpad Software; San Diego, CA).

Flow cytometry

Purified T cells stained with respective Abs were analyzed by three-color flow cytometry (FACScan II; BD Biosciences, San Jose, CA) to assess purity. Antibodies were incubated with whole-spleen single-cell suspension in PBS with 5% FBS, on ice for 30 min, followed by a wash with the PBS with 5% FBS. Subsequently, 100,000–300,000 flow events were acquired.

Gallyas silver staining

Gallyas silver stain was used to visualize fibrillar aggregates. Free floating brain sections were placed in 5% Periodic Acid for 3 min, washed twice and placed in Silver Iodide solution 1 min, followed by incubation in 0.5% Acetic Acid 5 min (2X), and rinsing with dH_20. Sections were incubated in developer for ~10 min until sections were pale brown/gray, and stopped in 0.5% acetic acid for 5 min, rinsed in dH_2O and mounted. Stained sections were examined by microscopy. Stained neurons were counted from CA2 of hippocampus, and their proportions within total neurons visually quantified in triplicate from entorhinal and cingulate cortex.

Neuronal counts

Whole-number neuronal estimates were performed using the optical fractionator method [27] with stereological software (Stereo Investigator; MBF Bioscience). Para-median sagittal serial sections spaced 50 µm apart were stained with NeuN. CA1, CA2, CA3 and other regions of interest were defined according to the Paxinos and Watson mouse brain atlas. A grid was placed randomly over the ROI, and cells were counted within three-dimensional optical dissectors (50 µm 50 µm 10 µm) using a 100x objective. Within each dissector, 1 µm guard zones at the top and bottom of section surface were excluded. Estimated totals weighted by section thickness were obtained with Stereo Investigator software, yielding a coefficient of error 0.10.

Behavioral testing - general

Open Field testing was performed preceding all other behavioral tests, at 3, 6, and 13 months post-cell or -control injection. Testing order was randomized by alternating control and treatment group animal runs. Testing started at the same time (+/- 1.5 hr) for tests run on more than one day, with early and late times alternated for inter-group randomization.

Open field test

Testing was carried out in an Open Field apparatus made up of an open topped, clear Plexiglas box, measuring 40.64 cm x 40.64 cm and 38.1 cm high. Two rings of photobeams and optical sensors surrounded the box. The optical sensors were connected to a computer by way of an input matrix. Each mouse was placed into the box, and beam interruptions were automatically recorded as a measure of locomotor activity. Each mouse was tested in the box for a period of 30 min.

Barnes maze test

Barnes Maze (BM) testing was performed a single time only, 14 months post-cell or –control injection. The BM test is a hippocampus-dependent, spatial-learning task that allows subjects to use spatial cues to locate a means of escape from a mildly aversive environment (i.e. the mice are required to use spatial cues to find an escape location). Mice were assessed for their ability to learn the location of an escape box over the course of 9 days in the BM apparatus [28,29]. The escape hole is constant for each mouse over the five training days. Each mouse was tested three times per day (3 trials) for 4 days, followed by no testing for 2 days, and re-testing on day 7. A 35-60 min inter-trial interval separates each trial. Each trial began by placing one mouse inside a start box with a bottomless cube positioned centrally on the maze. After 30 seconds, the start box was lifted and the mouse was released from the start box to find the one hole with access to the escape box. Two fluorescent lights located approximately 4 feet above illuminated the testing room. Each trial lasted up to 4 min or until the mouse entered the escape box. The experimenter guided mice that failed to find the escape hole within 4 min, to the correct hole after each training test. Once the mouse entered the escape box, it was allowed to remain in the box for 1 min. Following the 7th day of testing, and never on the same day, mice were tested an additional two-days, in which the escape box was placed in the reverse position on day 8, and replaced in the original position on day 9. The same exact testing procedure was applied to all mice in all groups. The maze and all compartments were cleaned thoroughly with isopropyl alcohol to remove any olfactory cues after each trial, and prior to each day of testing. Additional randomization of alternating escape compartment location between each animal per group, and between each of 3 daily training tests per animal, was employed for this test.

Y-maze spontaneous alternation behaviour

519 Mice were tested for SA a single time only, at 12 months post-cell or –control injection. Y-
520 Maze Spontaneous Alternation Behaviour (SAB) is used to assess working memory. SAB was
521 measured by individually placing animals in one arm of a symmetric Y-maze made of opaque
522 black acrylic plastic (arms: 40 cm long, 4 cm wide; walls: 30 cm tall), and the sequence of arm
523 entries and total number of entries recorded over a period of 8 min.

524 ***Flinch-jump/fear conditioning tests***

525 Flinch-jump/Fear Conditioning freezing times were determined 6 and 11 months post-cell or
526 –control injection. We first determined there were no significant differences in the nociceptive
527 threshold (pain sensitivity) across treatment groups using the Flinch-Jump Test. Pavlovian Fear
528 Conditioning was then used to assess learning and memory regarding aversive events. The
529 apparatus (Freeze Monitor™, San Diego Instruments, San Diego, CA) consisted of a Plexiglas box
530 (25.4 x 25.4 x 31.75 cm high) with a stainless-steel grid floor. An acoustic stimulus unit is located
531 on top of the box, and the box is ringed with photo beams and optical sensors. The optical sensors
532 were connected to a computer by way of an input matrix, and the number of beam interruptions is
533 automatically recorded. For testing, on day 1 individual mice were placed into the test box, and
534 allowed to habituate for 3 min. At 3 min a tone was presented for 30 sec. Then, 30 sec after
535 termination of the tone, a 0.5 sec foot shock (intensity = mean jump threshold for the treatment
536 group determined by the Flinch-Jump Test) was delivered. The mouse was then removed from the
537 box and returned to its home cage for 2 min. The chamber was cleaned and the animal returned to
538 the chamber where the procedure was repeated. The freeze monitor apparatus recorded freezing
539 times throughout the procedure (absence of movement for 5+ seconds, resulting in no beam
540 breaks). On day 2, context retrieval was determined by placing the mouse into the same test box
541 where it previously received a tone and foot shocks, but here the tone and foot shocks were not

presented. Freezing time was measured over a 10-min period. On day 3, cue conditioning was measured after inserting a triangular, plexiglass box into the test box. The mouse was placed into the triangular chamber where they had not previously received tone or foot shocks, but after 1 min the auditory tone was delivered for 30 sec and freezing time measured for 10 min.

Human Subjects

Cohort 1: 40 control individuals (CTRL; normal aging – normal CSF profile; 16M, 24F; avg age 60.2 yr [49-88]); 52 MCI patients with an AD-characteristic CSF biomarker profile (MCI-AD; 20M, 32F; avg age 75.5 yr [49-88]); 36 MCI patients not displaying an AD-characteristic CSF biomarker profile (MCI; 17M, 19F; avg age 62.22 yr [42-82]); 50 sporadic AD patients with an AD-characteristic CSF biomarker profile (AD; 26M, 24F; avg age 76.08 yr [57-88]). AD biomarker positivity (in-house validated cut-off values of biomarkers were applied: $A\beta_{1\text{-}42}$ <638.5 pg/mL, T-tau>296.5 pg/mL, P-$tau_{(181P)}$ >56.5 pg/mL) was determined by means of commercially available single-analyte ELISA kits (INNOTEST® β-AMYLOID (1-42), INNOTEST® hTAU-Ag, and INNOTEST® PHOSPHO-TAU (181P); Fujirebio Europe). CSF samples were collected at Middelheim General Hospital (Antwerp, Belgium) and centers referring to the Neurobiobank of the Institute Born-Bunge (NBB-IBB; n° BB190113) according to standard collection protocols as described previously [30]. CSF was obtained by lumbar puncture (LP) at the L3/L4 or L4/L5 interspace. CSF samples were collected in polypropylene vials (Nalgene cat.no.5000–1020 (1.5 mL) and 5000–0050 (4.5 mL)), immediately frozen in liquid nitrogen, and subsequently stored at –80°C until analysis.

In addition, blood samples following venepuncture were collected after LP, of which 2-3 serum, 3-4 plasma and 2-3 total blood aliquots were stored (1.5mL for each aliquot).

MCI patients underwent LP at baseline as part of their diagnostic work-up. The inclusion criteria for the control group were: [1] no neurological or psychiatric antecedents and [2] no organic disease involving the central nervous system following extensive clinical examination. MCI patients were diagnosed applying Petersen's diagnostic criteria [31], i.e., [1] cognitive complaint, preferably corroborated by an informant; [2] objective cognitive impairment, quantified as performance of more than 1.5 SD below the appropriate mean on the neuropsychological subtests; [3] largely normal general cognitive functioning; [4] essentially intact activities of daily living (basic and instrumental activities of daily living were determined by a clinical interview with the patient and an informant); and [5] not demented [32]. AD dementia was clinically diagnosed according to the NINCDS/ADRDA and IWG-2 criteria [33] APOE allele status was 40% 3/4, 40% 4/4, 10% 3/3, 10% 2/4 for AD group (10 tested/50 total); 55% 3/4, 20% 4/4, 15% 3/3, 10% 2/4, 0% 2/3 for MCI-AD group (20 tested/52 total); 31% 3/4, 0% 4/4, 46% 3/3, 8% 2/4, 15% 2/3 for MCI-normal group (13 tested/36 total); 22% 3/4, 0% 4/4, 68% 3/3, 0% 2/4, 8% 2/3 for control group (37 tested/40 total). Mean MMSE score was 20 (5-29) +/- 5 for AD group (48/50 tested); 24 +/- 3 (15-30) for MCI-AD group (51/52 tested); 26 +/- 3 (18-30) for MCI-normal group (33/36 tested); 28 +/- 4 (17-30) for control group (9/37 tested). All included subjects were of Caucasian ethnicity.

Cohort 2: Cognitive Testing. 29 self-referred memory clinic patients (average age 49; 22-70) from Cedars-Sinai Dept. of Neurosurgery were clinically diagnosed as normal (n = 6), MCI (n = 18), dementia (n = 3), or uncertain (n = 2; diagnosis established solely on basis of cognitive testing), and followed up with cognitive (Montreal Cognitive Assessment; MoCA) testing (n = 22). Cognitively normal = MoCA score 29-30; age-related cognitive decline = MoCA score 26-28;

MCI = MoCA score < 26. HLA-A2-negative patients were determined by flow cytometry and excluded from analysis, as were patients with $\leq$2.5% $CD8^+$ cells in lymphocyte gates.

Cohort 3: Brain Western and IHC. Hippocampal lysates from 13 autopsy-confirmed Braak stage IV (n = 4) and Braak stage V-VI (n = 9) sporadic AD patients, and 5 age-matched normal controls were run on Western blots using anti-CD8 or anti-PRF1. Hippocampal sections from 10 autopsy-confirmed Braak stage V-VI sporadic AD patients, and 10 age-matched normal controls were stained with anti-CD8-flourescein plus $APP_{(471-479)}$/HLA-A2-PE. HLA-A2-negative samples were not excluded from Western and IHC/IF analysis.

Statistical analysis

Quantification and stereological counting procedure for cell numbers or area (μm^2) of Aβ plaque, $GFAP^+$, $Iba1^+$ or $Perforin1^+$ cells were analyzed in six to eight coronal sections from each individual, at 150-µm intervals (unless otherwise indicated), covering 900–1200 µm of the hippocampal and cortical areas. Specific fluorescence signal was captured with the same exposure time for each image and optical sections from each field of the specimen were imported into NIH Image J and analyzed as above. GraphPad Prism (version 5.0b; San Diego, CA, USA) was used to analyze the data using ANOVA and T-Tests with Welch's correction (no assumption of equal variance). In all histograms, average $\pm$ SEM is depicted.

Data from Open Field and Barnes Maze tests were analysed by 2-sided T-Test for individual test points, and by ANOVA on test curves, when normal distribution/$P > 0.05$ of data was verified in Anderson-Darling, D'Agostino & Pearson, Shapiro-Wilk, and/or Kolmogorov-Smirnov tests. 1-sided T-Test was used to analyze Y-maze/SAB. Mann Whitney test was substituted for T-Tests when non-normal distribution/$P < 0.05$ was indicated in Anderson-Darling, D'Agostino & Pearson,

Shapiro-Wilk, and/or Kolmogorov-Smirnov tests. Flinch-Jump and Fear Conditioning Tests was normalized, first within each group to the average of the initial two tests in training on day 1, and then within all experimental groups to the average contextual or cue values of PBS controls, expressed as percent of control, and analyzed by ANOVA, followed where appropriate by Newman-Keuls tests to detect differences among treatment groups.

Sample sizes for PrfKO-CD8 and IfnγKO-CD8 groups were calculated *a priori* for each metric using means and standard deviations of PBS and wt-CD8 groups for anticipated effect sizes, with alpha 0.05, and >95 confidence. Calculated n plus $\geq$1 were then used for PrfKO-CD8 and IfnγKO-CD8 groups.

Pre-determined exclusions included sections or samples with no discernible background signal, and values within each group $\geq$2 standard deviations above or below the median/group. Subject numbers and methods of reagent validation are shown in Table S1.

Study approval

All animal procedures were approved prior to performance by the Cedars-Sinai Institutional Animal Care and Use Committee. The Cedars-Sinai Institutional Review Board designated the analysis of de-identified human brain specimens from UC Davis exempt from committee review. Brain specimens were collected, stored, and disseminated with prior approval by the UC Davis Medical Center Institutional Review Board. Sampling for cohort 1 was approved by the Medical Ethics Committee of the Hospital Network Antwerp (ZNA), Antwerp, Belgium (approval number 2805 and number 2806).

Data Availability

Results and raw data will be made available upon request. Model Organisms and/or the means to generate them will be made generally available for research (non-commercial) use.

Acknowledgments:

We gratefully acknowledge support in conducting behavioral tests from the Cedars-Sinai Research Institute Biobehavioral Core, and Ms. Hannah Schubloom and Mia Oviatt for excellent administrative support and editing.

Author contributions:

AP performed Western blots, behavioral assays, mouse colony management, and flow cytometry; AR performed, analyzed, and quantified tissue immunostaining, and conducted neuronal counts; MJ performed Western blots, behavioral assays, and ELISAs; RMC provided guidance on model development and analysis, and evaluated the studies' relevance to human conditions; RC performed behavioral assays and mouse colony management; NY performed tissue immunostaining and mouse colony management; RNP designed and analyzed behavioral assays; GD performed Western blots; AM performed Western blots; DG performed flow cytometry; HS performed behavioral assays; L-WJ characterized and provided human brain specimens; DVD, YV, and HDR performed flow cytometry; PPDD characterized and provided human blood specimens, and advised on analysis; KLB evaluated the studies' relevance to human conditions; CJW designed all studies, coordinated experiments, analyzed and compiled all data, and wrote the manuscript.

Competing interest declaration:

CW is the author of patents PCT/US2016/049598, WO2017/040594, and PCT/US2019/017879. RC and KLB are co-authors on patent PCT/US2019/017879. PCT/US2016/049598, WO 2017/040594 is licensed by Cedars-SinaiMedical Center to T-Neuro Pharma, Inc. CW has received salary and ownership interest in T-Neuro Pharma, Inc.

Additional information:

Funding: This research was supported in part by UC Davis Alzheimer's Disease Center (P30 AG10129), NIH grants to RMC and CJW (R21NSO54162 and R21AG033394, respectively), a grant from the Joseph Drown Foundation (CJW), and the Maxine Dunitz Neurosurgical Institute.

Running Title: CD8 T cell aging in Alzheimer's pathology

Keywords: Alzheimer's Disease, CD8 T cell, immune aging, homeostatic expansion, neurodegeneration

Abbreviations: Alzheimer's disease (AD); Alzheimer's disease transgenic (ADtg); Amyloid Precursor Protein (App); beta-amyloid (Aβ); experimental autoimmune encephalomyelitis (EAE); familial Alzheimer's disease (FAD); Fear Conditioning (FC); hyper-phosphorylated tau protein (pTau); multiple sclerosis (MS); neurofibrillary tangles (NFTs); regions of interest (ROI)**;** Spontaneous Alternation (SA); T Cell Receptor beta (TCRVβ); paired-helical filaments (PHFs). Resident memory CD8 T cells (CD8 T_{RM}).

Supplementary information: found at https://mts-nature.nature.com/nature_files/2021/02/02/00394605/00/394605_0_data_set_3597679_qnw3pg.docx.

671 [2]Correspondence to C.J. Wheeler: chris@tneuropharma.com

672

Extended data figure legends

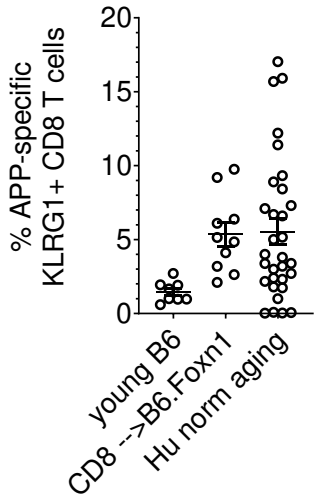

Fig. E1: Flow cytometry and Western analysis of T cell and amyloid markers. Levels of mouse $APP_{(470-478)}$/H-$2D^b$ and human $APP_{(471-479)}$/HLA-A2 were quantified within $KLRG1^+$ CD8 T cells by flow cytometry in mouse and human blood, respectively. Young B6 = APP-reactive T cells within splenic lymphocytes from 8-10 week-old C57BL/6 females; CD8 → B6.Foxn1 = APP-reactive T cells within splenic lymphocytes from 10-12 week-old B6.Foxn1 female recipients of purified CD8 T cells from 6-8 week-old C57BL/6 females 3-5 weeks prior; Hu norm aging = APP-reactive T cells within peripheral blood lymphocytes of neurodegenerative disease-free human subjects aged 49-88 years, whose values also appear in Fig. 4c.

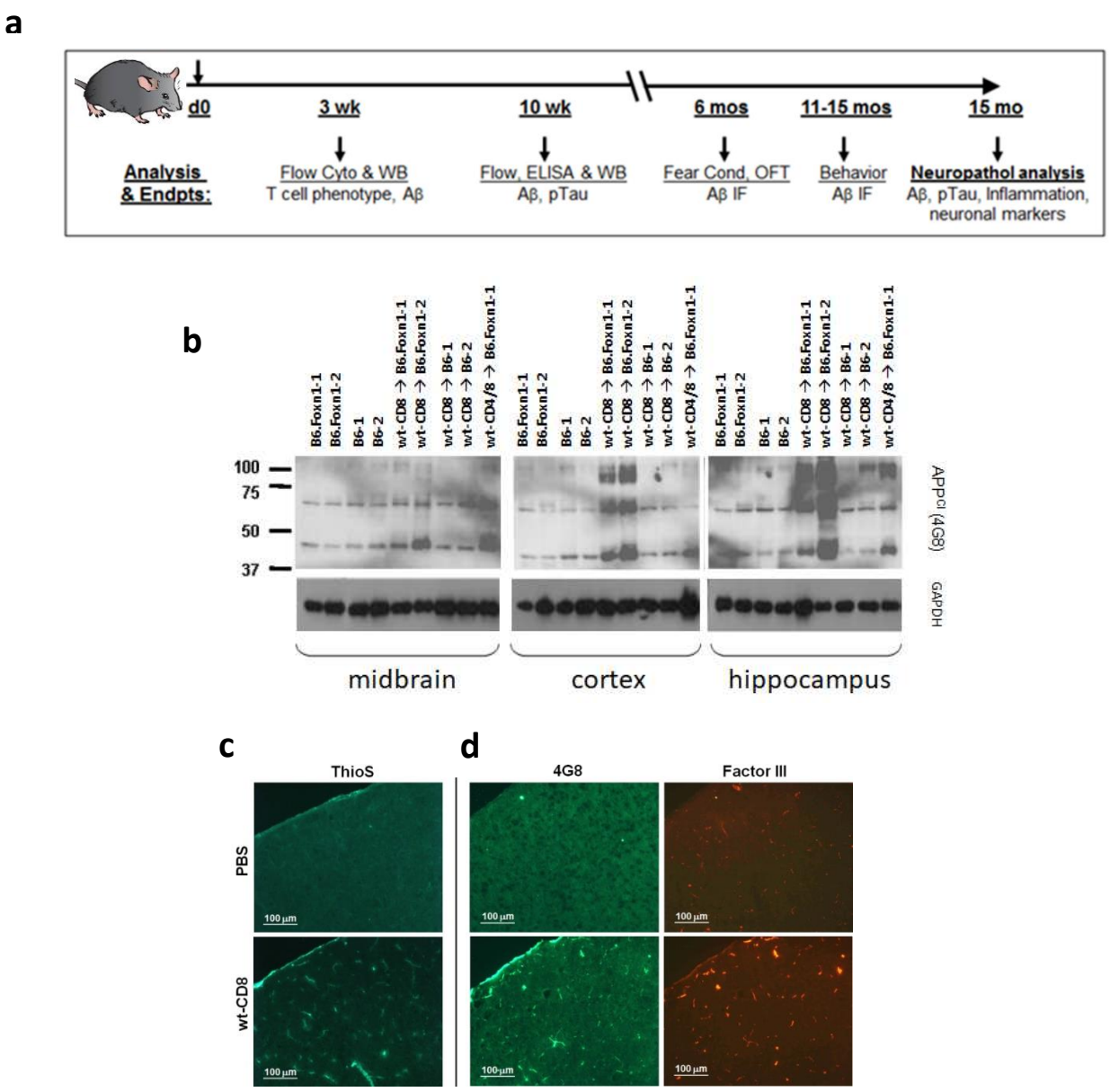

Fig. E2: Analysis scheme, APP cleavage products, and vascular Aβ in brain after T cell injection. Analysis time line in CD8 T cell-injected B6.Foxn1 recipients (**a**). Western analysis of APP cleavage products/Aβ oligomers (APP^{Cl}) with 4G8 antibody in dissected regions of mouse brain 10 weeks after injection with 3 x 10^6 purified T cells. CD4/8 indicates injection of ~85% CD4 and 15% CD8, with peripheral proportions verified by flow cytometry (**b**).

Immunohistochemical staining for ThioS in B6.Foxn1 cortex 6 months post-injection, exhibiting vascular staining pattern in wt-CD8 T cell-injected, but not PBS-injected mice (**c**). Aβ (4G8) and Factor III staining in B6.Foxn1 cortex 6 months after injection, confirms deposits of aggregated vascular Aβ in nude mice harboring ^{hi}T cells (**d**). All images at 5x magnification.

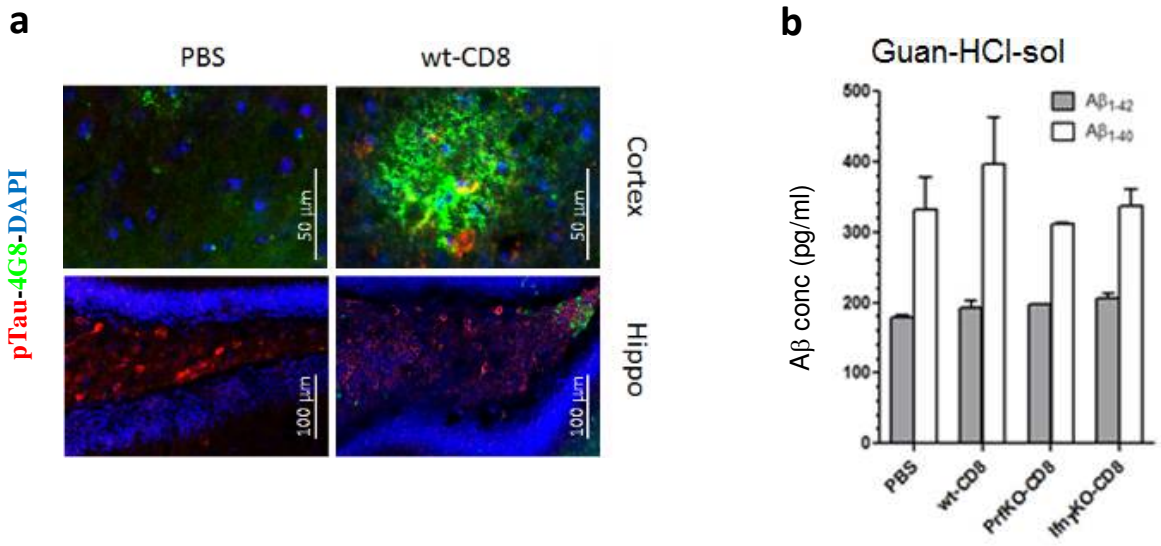

Fig. E3: Aβ accumulation in nude mouse brain after CD8 T cell injection. Representative example of individual Aβ ($4G8^+$) plaque morphology within entorhinal cortex and hippocampus in nude recipients 15 months after CD8 T cell injection. Magnification and image acquisition parameters were identical within each brain region **(a)**. Forebrain ELISA of GuanidineHCl-soluble Aβ in B6.Foxn1 brain 15 months after CD8 T cell or control injections **(b)**.

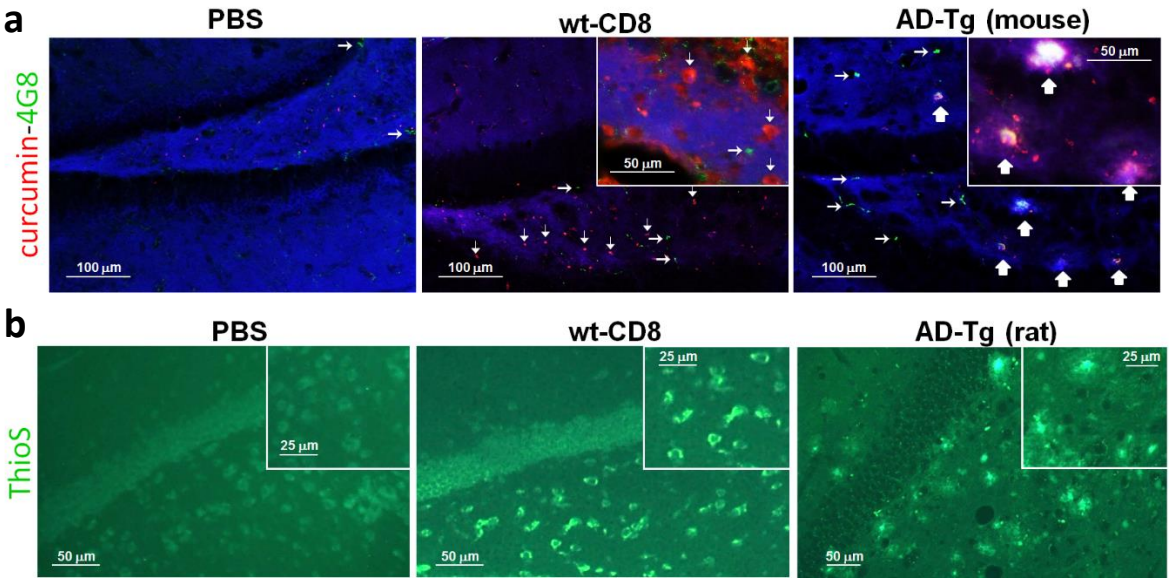

Fig. E4: Distinct curcumin and ThioS staining in dentate gyrus of nude mice harboring hiT cells. a, Hippocampal sections from the indicated groups (all B6.Foxn1 recipients, except AD-Tg = Tg2576 mice), were stained for 4G8 (Aβ) and curcumin, 6 months after i.v. control/cell injection, or at 14 months of age for AD-Tg (**a**). Right-facing arrows highlight Aβ deposits with no curcumin co-staining. Up-facing arrows depict co-localized Aβ and curcumin deposits, representing mature neuritic plaques. Down-facing arrows highlight curcumin^{+} structures with no Aβ co-staining, i.e., non-amyloid fibrillar deposits. No DAPI was used in the stains; blue channel background is provided for anatomical context only. Follow-up ThioS staining of PBS and wt-CD8 group B6.Foxn1 hiT recipients 6 months after control/cell injection, and 20 month-old AD-Transgenic (Tg) rat dentate gyrus (**b**). Rat AD-Tg brain was used due to its explicit Tau PHF content (Cohen et al., 2013), that nevertheless failed to stain with ThioS in our hands.

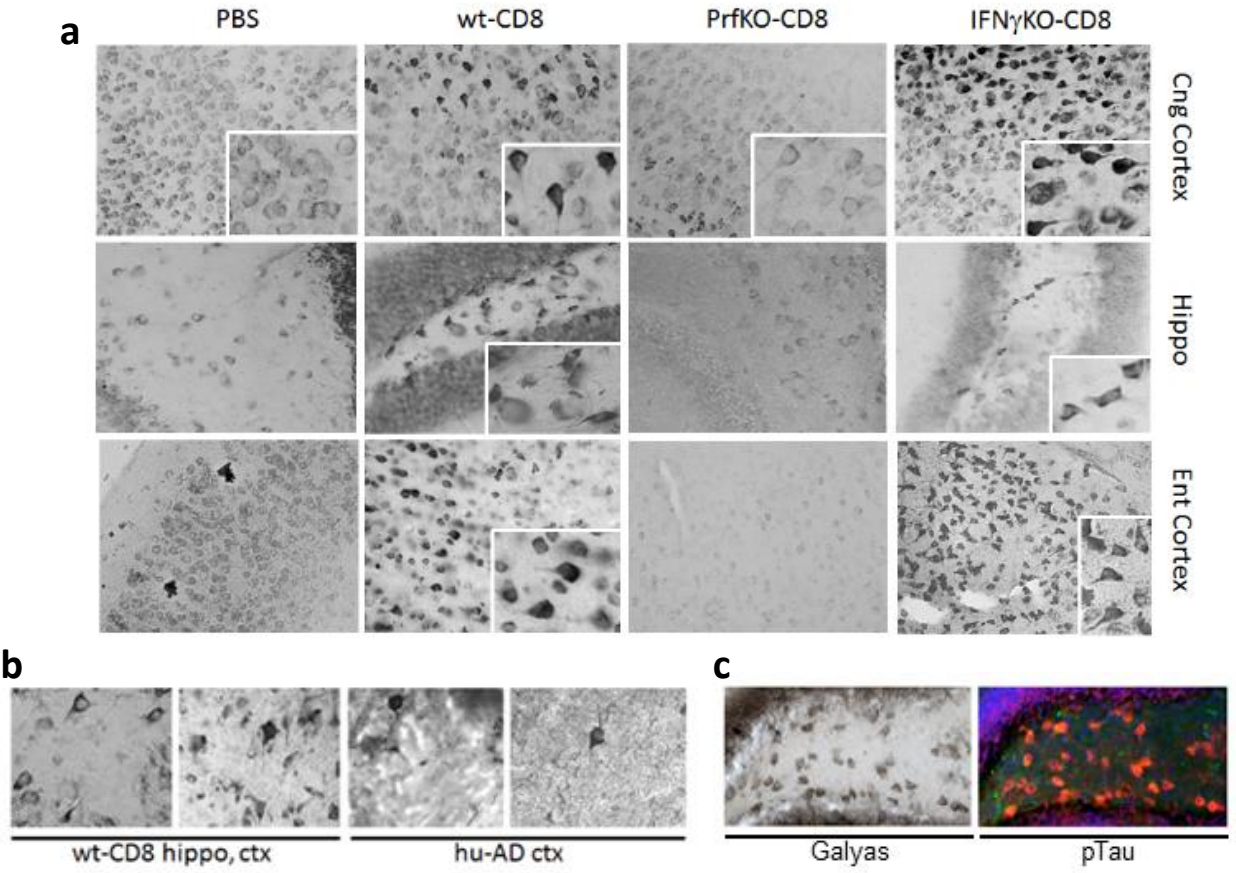

Fig. E5: Silver stained neuronal structures in experimental groups. Gallyas silver staining of cortical and hippocampal brain regions, showing typical neurofibrillary tangle (NFT) morphology in wt-CD8 and IFNγKO-CD8 group mice (insets). Background silver staining was occasionally evident in PrfKO-CD8 or PBS group mice, but did not exhibit similar NFT morphology (insets). Individual images were derived from different mice within each group (**a**). Comparison of Gallyas^{+} structures in nude mice harboring ^{hi}T cells (wt-CD8) hippocampus (left) and cortex (ctx, right), to those in cortex of human severe AD (Braak stage VI; **b**). Sequential staining of wt-CD8 group mouse hippocampus reveals identical staining pattern between Gallyas and pTau, but not Gallyas and 4G8/Aβ (**c**). Magnification and scale are identical for all images (20x), and among insets in **a**.

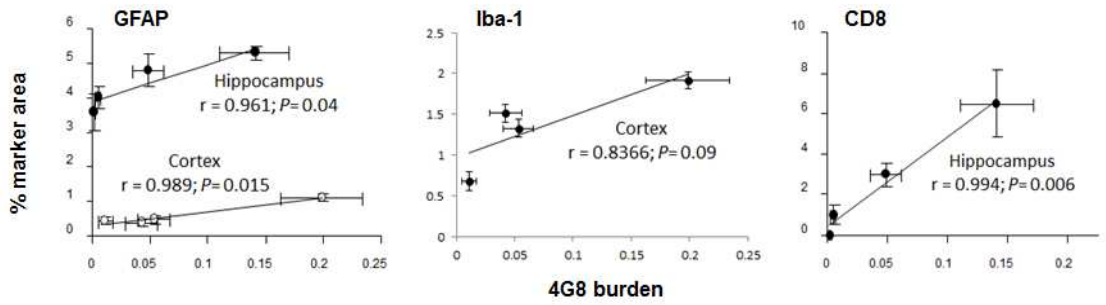

Fig. E6: Innate and adaptive immune correlates of amyloidosis in nude mice harboring hiT cells. Brain was co-stained for CD8 and pTau (inset), and quantified within hippocampal and cortical brain sections from B6.Foxn1 recipients 15 months after injection of wild-type, IFNγKO or PrfKO CD8 T cells, or PBS as previously reported (Panwar et al., 2020; reference 7 in manuscript). Group data are compiled for Astrocytic (GFAP), microglial (Iba-1), and CD8 T cell (CD8) areas were correlated with $4G8^+$ plaque burden within each group, with *P* values of linear regressions and Pearson's correlations (r) shown (**C**). Numbers of mice per group are listed in Supplemental Table 1.

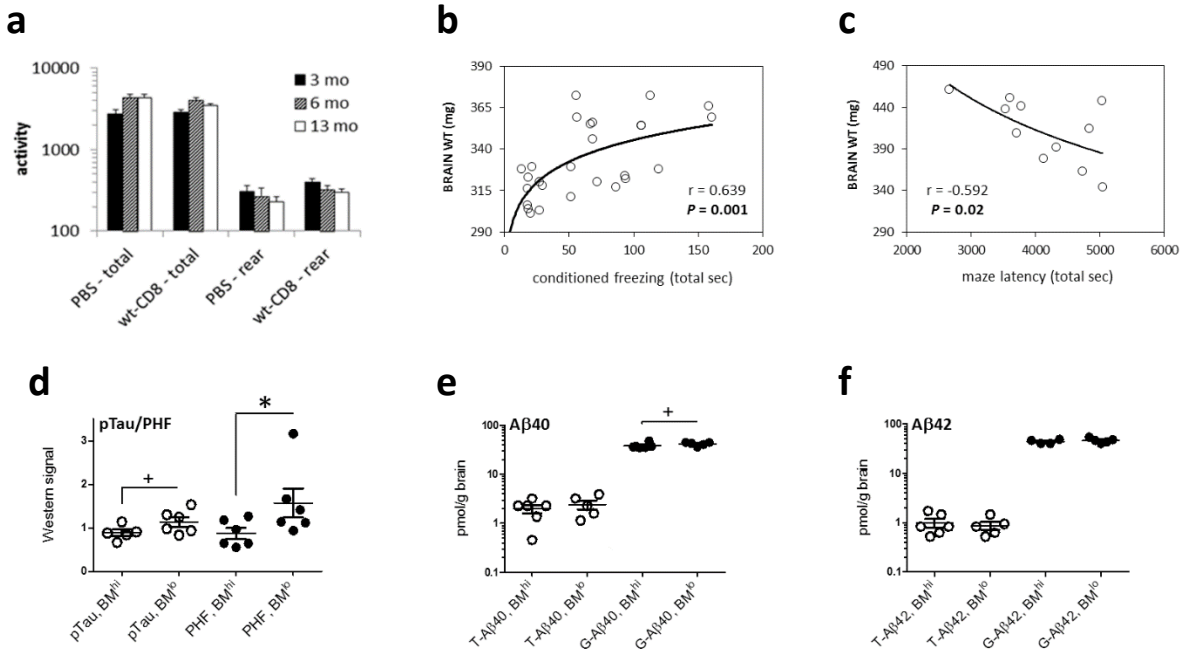

Fig E7: Motor activity, cognitive performance and correlation with pathological features. Open Field total activity and rearing activity at 3, 6, and 13 months post-injection of CD8 T cells in experimental mouse groups (**a**). There was no substantial alteration in total or rearing activity between PBS and wt-CD8 groups at any time point, although total activity significantly increased after 3 months, and rearing activity significantly decreased by 13 months, in both groups ($n \geq 9$ mice/group). Individual mouse performance in Fear Conditioning test at 6 months correlated directly with brain mass ($n = 27$; mice were from PBS and wt-CD8 groups; **b**). Superior performance of individual mice in Barnes Maze at 14 months was significantly associated with higher brain mass ($n = 9$; mice were from all groups; $^{*}P > 0.05$, $^{+}P > 0.1$ by 2-tailed T-test; **c**). Stratification by median latency in Barnes Maze correlated significantly with Tau PHF only (**d**), although marginal non-significant trends were observed for pTau and GuanidineHCl-soluble Ab40 relative to Triton X-100-soluble Aβ species (G-Aβ and T-Aβ, respectively; BM^{hi} = longer latency; BM^{lo} = shorter latency; **e, f**).

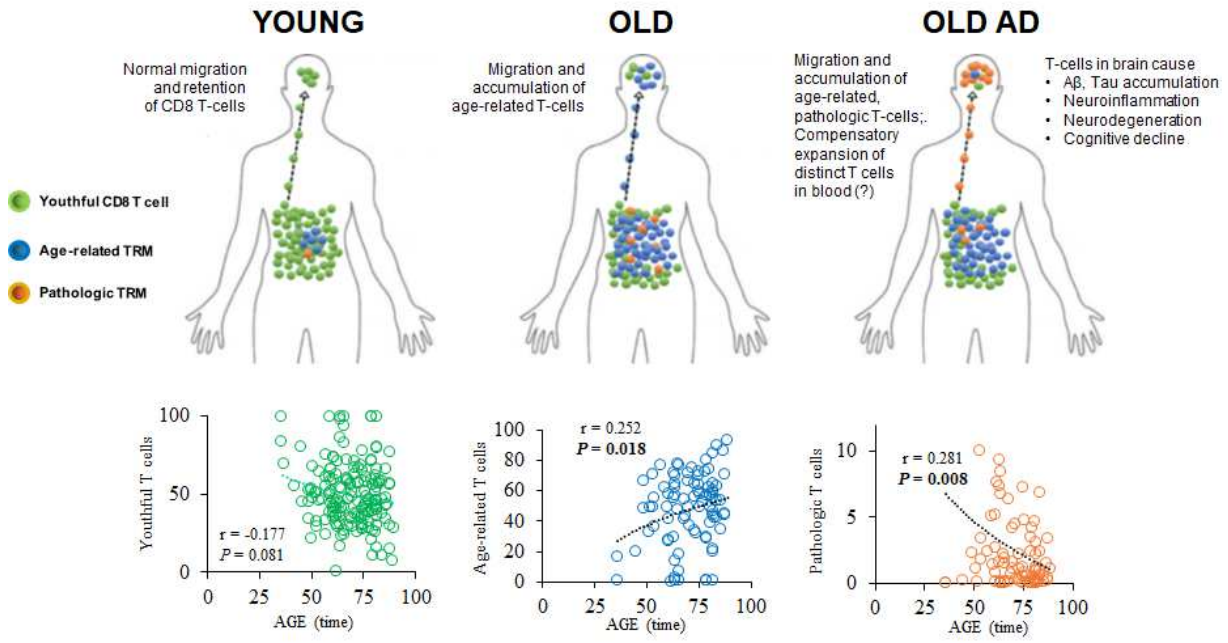

Fig. E8: KLRG1$^-$ ("youthful"), KLRG1$^+$ ("age-related"), and APP$_{(471-479)}$/HLA-A2 multimer-reactive KLRG1$^+$ ("pathologic") CD8 T cells exhibit differential associations with age. Whole blood from 165 human patients (31 MCI – norm bio; 45 MCI – AD bio; 40 normal aging controls; 49 AD) was analysed by flow cytometry for KLRG1$^+$ and KLRG1$^-$ CD8 T cell content in lymphocyte gates, and plotted relative to patient age at blood collection, with APP$_{(471-479)}$/HLA-A2 multimer reactivity within KLRG1$^+$ CD8 T cells further quantified in the subset of 88 HLA-A2$^+$ patients. Possible migration of age-related and APP-reactive T cell subsets from blood to brain as depicted above the plots is proposed.

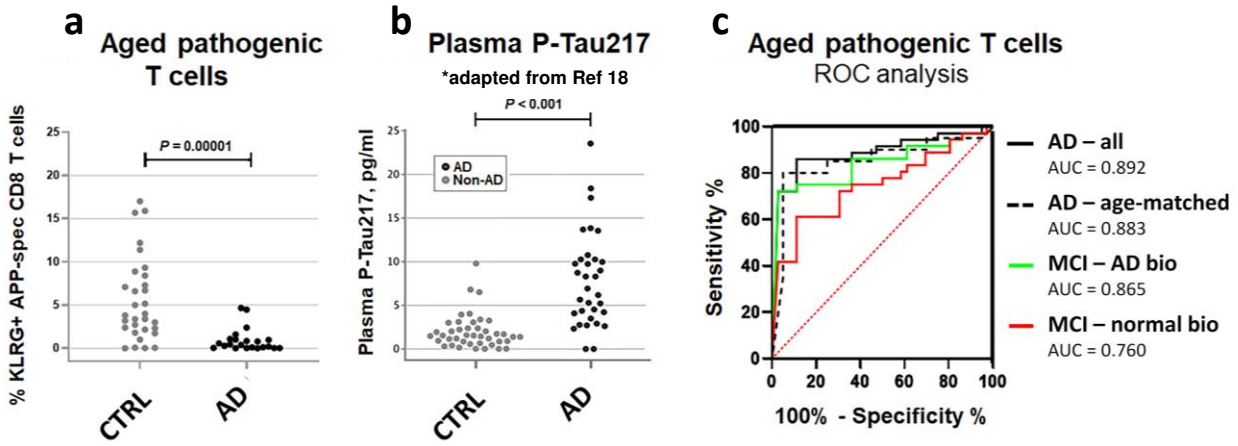

Fig. E9: Comparison with P-Tau217 and receiving operator characteristic (ROC) curves for APP-specific KLRG1$^+$ CD8 T cell level in human patients. Levels of APP/HLA-A2 multimer-reactive KLRG1$^+$ CD8 T cells in blood of AD patients from our study (**a**) relative to published plasma levels of P-Tau217 (Palmqvist et al., 2020. JAMA 324(8):772-781; **b**). Receiver Operating Characteristic (ROC) plots of APP/HLA-A2 multimer-reactive KLRG1$^+$ CD8 T cells in blood of indicated patient cohorts relative to normal aging controls (**c**) Mild Cognitive Impairment without (MCI-normal bio) and with (MCI-AD bio) CSF biomarkers consistent with AD, and confirmed AD patients ages 57-84 (AD-all). Area Under the Curve (AUC) is indicated. AD-age-matched indicates ROC analysis on 10 AD patients for whom precisely age-matched controls were available (+/- 1 year; n = 10). $P < 0.001$ for all curves except MCI – normal bio ($P = 0.003$).

Figures

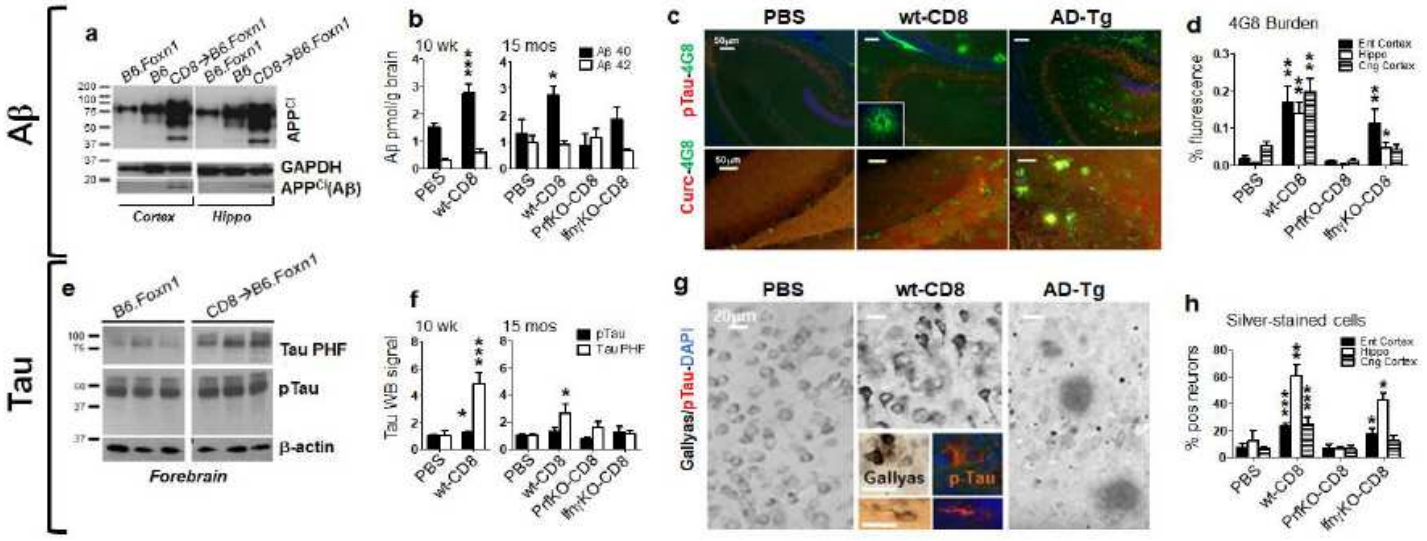

Figure 1

Amyliod and pTau pathology. Western blots of APP cleavage products (APPCl) in cortex, hippocampus 3 wk after injection (□) of recipients (a). B-J depict B6.Foxn1 recipients , 15 mos post-injection unless otherwise indicated. Forebrain Aβ1-40/42 ELISA (b). Plaques + pTau/curcumin staining (c), and compiled 4G8 burden in entorhinal (Ent)/cingulate (Cng) cortex, and hippocampus (Hippo) (d). Western blots (e), and compiled pTau and PHF signal. Gallyas/silver-stained cells in hiTRM groups and 18-month-old Tg2576 (AD-Tg) mice, with sequential pTau□Gallyas stains inset (g). Gallyas+ neuron (h) percentages Plots depict averages + SEM. *P < 0.05, **P < 0.01, ***P < 0.005 by 2-sided T-test, relative to PBS group.

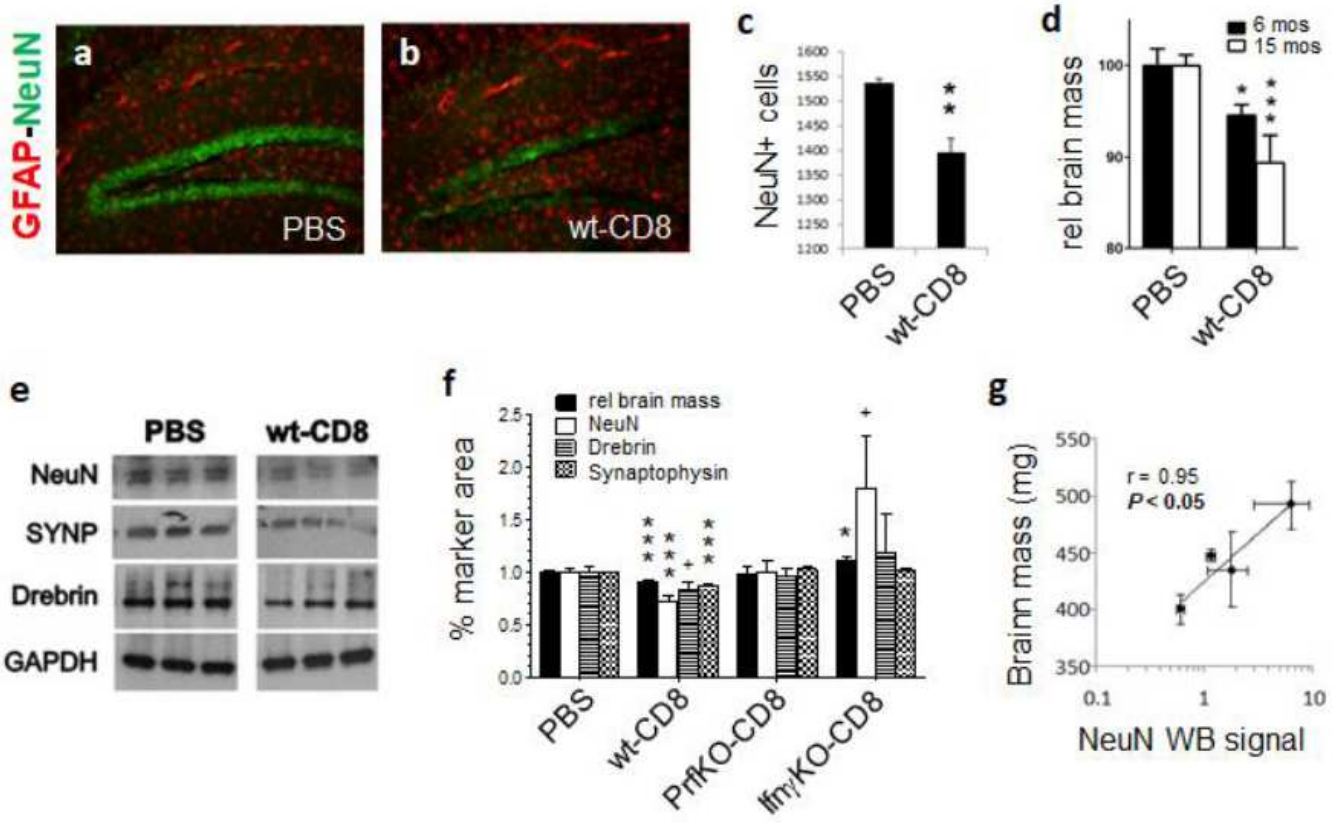

Figure 2

Neurodegeneration in nude mice harboring hiT cells. Cell/control recipients in all panels are B6.Foxn1 exclusively. NeuN and GFAP staining (a, b), and cell counts in hippocampus, 15 mos after cell/control injection (c). Brain atrophy over time in PBS and wt-CD8 groups (mass normalized to PBS controls at each time point; d). Representative forebrain Westerns (e), and GAPDH-normalized NeuN, Drebrin, and Synaptophysin Western signals (f). Correlation of NeuN with brain weight (g). Plots depict averages + SEM. *P < 0.05, **P < 0.01, ***P < 0.005 by 2- sided T-test, relative to PBS group.

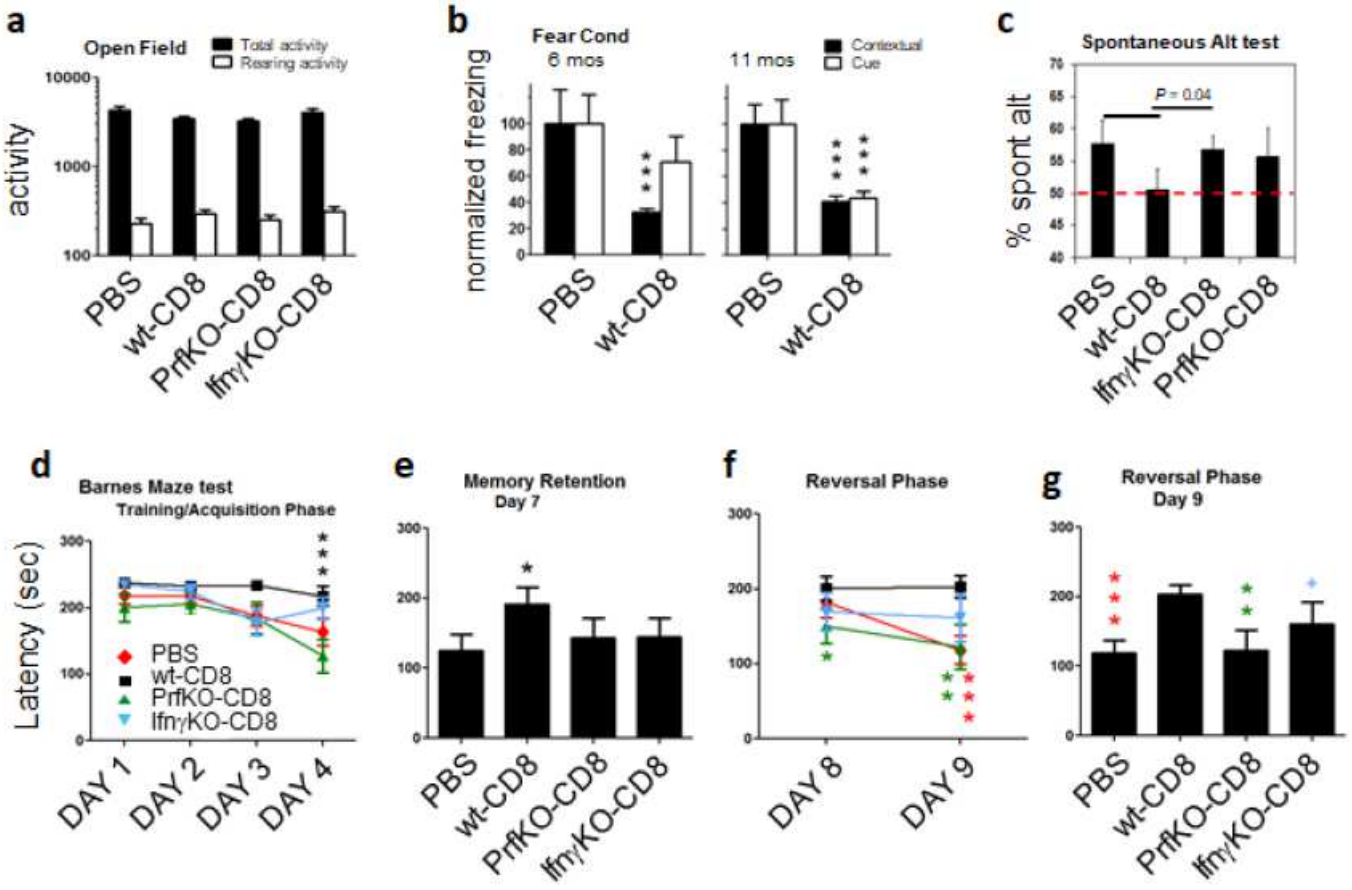

Figure 3

Cognition in nude mice harboring hiT cells. Representative Open Field test at 13 mos (a). Fear Conditioning over time (b), and Spontaneous Alternation Behavior at 12 months (c). Barnes Maze learning/training (d), retention (e), and reversal (f, g) phases, at 14 mos (black, colored symbols = P relative to PBS, wt-CD8, respectively). Plots depict averages + SEM. *P < 0.05, **P < 0.01, ***P < 0.005 by 2-sided ANOVA (panel d) or 2-sided T-test (all others), relative to PBS group unless otherwise indicated.

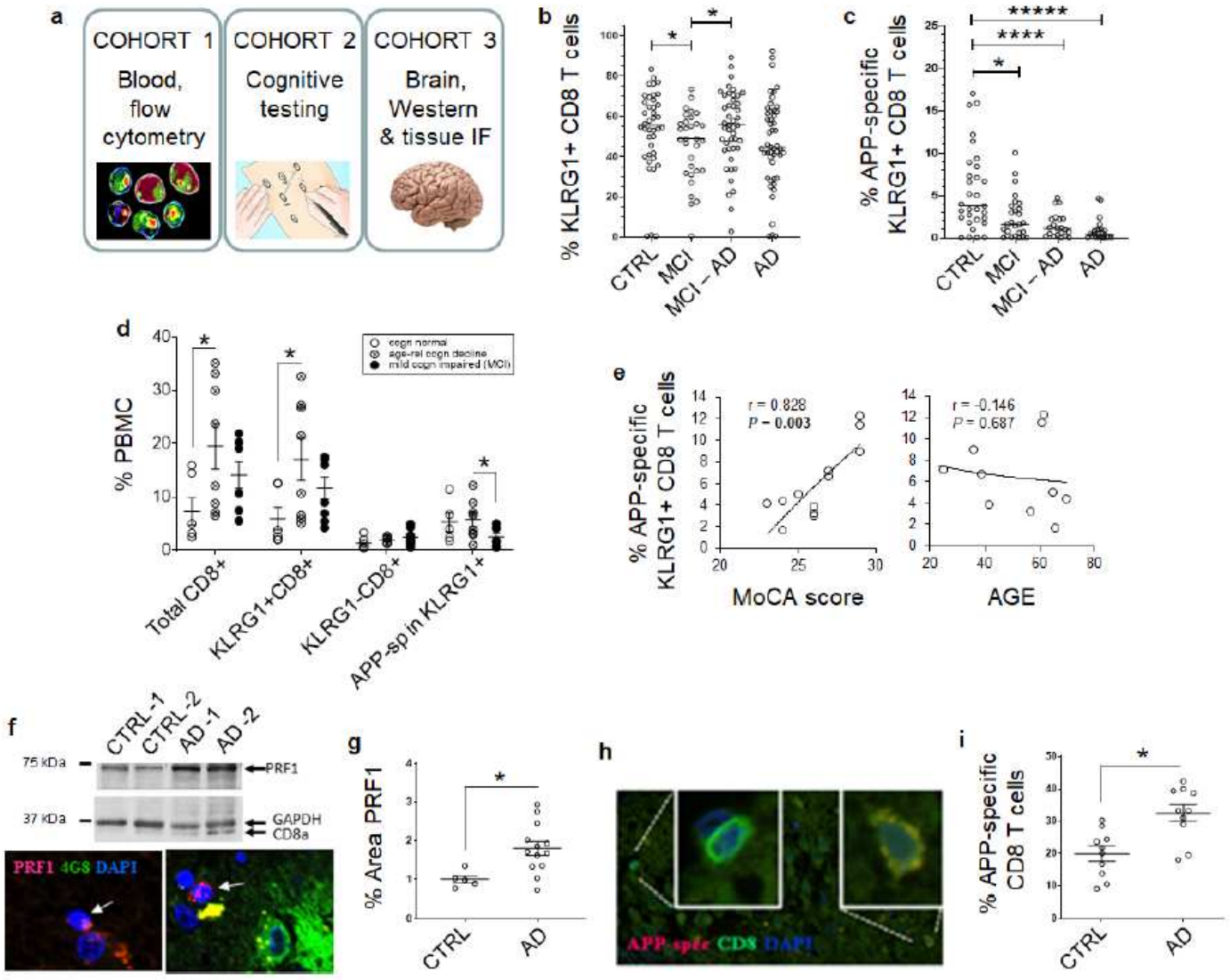

Figure 4

hiT parameters in human Alzheimer's. Patient cohorts (a). KLRG1+ (b) and APP(471- 479)/HLA-A2-reactive KLRG1+ (c) CD8 T cells in CTRL, MCI + CSF AD biomarkers (MCI, MCI– AD), and verified Alzheimer's (AD) blood. T cell subpopulations vs. MoCA score (d), and correlation of APP(471-479)/HLA-A2-reactive KLRG1+ CD8 with score and age (e). PRF1 Western blot and immunofluorescence (f), with quantifications in age-matched CTRL and AD brains. (g). APP(471-479)/HLA-A2-reactive CD8 staining (h) and quantification (i) in brain. Plots depict averages + SEM. *P < 0.05, **P < 0.01, ***P < 0.005, ****P < 0.001 by 2-sided T-test, relative to CTRL unless otherwise indicated.

Supplementary Files

This is a list of supplementary files associated with this preprint. Click to download.

- NatureSupplementalInformationclean12520b.docx